Radon Gas Detection via Vegetation Spectra Responses Using Space-borne Remote Sensing: A Tool for Uranium Exploration

A Thesis Submitted to the College of
Graduate and Postdoctoral Studies
In Partial Fulfillment of the Requirements
For the Degree of Master of Science
In the Department of Geography and Planning
University of Saskatchewan
Saskatoon, Canada

By

Kristin Martin

PERMISSION TO USE

In presenting this thesis in partial fulfillment of the requirements for a graduate degree from the University of Saskatchewan, I agree that the Libraries of this University may make it freely available for inspection. I further agree that permission for copying of this thesis in any manner, in whole or in part, for scholarly purposes may be granted by the professor or professors who supervised my thesis work or, in their absence, by the Head of the Department or the Dean of the College in which my thesis work was done. It is understood that any copying or publication of use of this thesis or parts thereof for financial gain shall not be allowed without my written permission. It is also understood that due recognition shall be given to me and to the University of Saskatchewan in any scholarly use which may be made of any material in my thesis.

Requests for permission to copy or make to other use of material in this thesis in whole or part should be addressed to:

Head of the Department of Geography and Planning
117 Science Place
University of Saskatchewan
Saskatoon, Saskatchewan S7N 5C8 Canada

OR

Dean
College of Graduate and Postdoctoral Studies
University of Saskatchewan
116 Thorvaldson Building, 110 Science Place
Saskatoon, Saskatchewan S7N 5C9, Canada

ABSTRACT

This research aims to determine if there is a discernable satellite-derived spectral signature within vegetation communities that can be linked to elevated occurrences of radon gas. Radon surveys, where the gas is measured directly on the ground, are a tool used in uranium exploration as statistically significant elevated radon values are known to occur in proximity to uranium mineralization. To-date, there has been little to no research into the use of optical remote sensing to quantify radon gas in uranium exploration. Through digitizing and geo-referencing historic survey data from Cluff Lake, Saskatchewan, the radon values were first explored along environmental gradients to understand its spatial distribution. The data were then linked with satellite imagery (Sentinel-2A) to explore spectral patterns and evaluate the potential of characterizing a spectral response that can highlight areas containing above background gas concentrations. Results show that there is strong potential for mapping radon gas via changing spectral characteristics within vegetation, interpreted to be attributed to the effects of radiogenic stress and metal contamination within plants coinciding with anomalous radon gas occurrences and/or elevated amounts of its progeny. It is shown that there are differences in spectral curves of natural-logarithmically transformed radon point-values that have been grouped based on standard deviation between what is considered background, moderate, and high values of radon. Furthermore, vegetation indices using Sentinel-2A bands, focusing in the red-edge and NIR portion of the electromagnetic spectrum, show a significant variation of means between grouped radon values allowing for trend detection and radon pseudo-survey map generation. Investigation into radon distribution at Cluff Lake has also shown a potentially significant relationship between radon gas and vegetation communities, specifically black spruce (*Picea mariana*), which was not hypothesized. The potential species specific relationship between radon gas and vegetation, along with the variation in spectral curves differentiating what is considered background and elevated occurrences of the gas, show strong potential for further refining radon pseudo-survey maps based on spectral characteristics of the tree-canopy. This research was designed as a tool in uranium exploration, to compliment geological, geophysical, and geochemical exploration methods. The research also has trans-disciplinary applications in biogeochemistry, ecology, and the environmental sector as an aid in mapping radiogenic contamination.

ACKNOWLEDGMENTS

I would like to thank Orano Canada Inc. for allowing the use of their data and for allowing me to pursue this research, in particular, P.Ledru, C.Cutts, D. Quirt, and R. Roy. I would also like to acknowledge all of my colleagues at Orano Canada Inc. who have provided encouragement throughout my MSc program.

I would like to extend my thanks to my supervisor, Dr. Xulin Gou, and my committee Dr. John Wilmshurst and Dr. Dirk De Boer for their guidance throughout this project. Xulin and John have made valuable edits and contributions to this study and I am very appreciative of their assistance and direction.

Additionally, the DigtalGlobe Foundation has generously provided WorldView imagery data which I am grateful for as it added value to this work.

TABLE OF CONTENTS

LIST OF TABLES

LIST OF FIGURES

1 Introduction

The field of remote sensing has valuable applications in mineral exploration, especially as technological advancements allow for mapping at higher spatial and spectral resolutions. Conventional methods for uranium exploration include magnetic, gravity, and resistivity geophysical surveys as well as analysis of geochemical and geological data derived from drilling. Uranium exploration is challenging; success largely relies on overlapping a multitude of data sets to aid in targeting and locating discrete pods of uranium mineralization that occur anywhere from just below the surface to depths of hundreds of meters.

Radon surveys are an additional tool in uranium exploration as the gas is a mobile product within the uranium-thorium decay chain. Broadly speaking, radon is able to travel through uranium fertile-fault zones that propagate to the surface. Current survey methodologies rely on the direct detection of the gas at the earth's surface; the indirect investigation of the effects of radon within vegetation using optical remote sensing has not yet been examined. As this is a new application of the discipline, many research gaps on the topic exist.

This project uses an entirely inductive research approach based on the assumption that there is a spectral signal linked with radon gas that can be mapped within vegetation communities using optical remote sensing approaches. The research is data-driven and provides a first pass assessment of the potential for the indirect detection of radon via remote sensing from a satellite platform. Additionally, the project provides a synthesis of trans-disciplinary research which is pivotal for refining and developing the technique further.

2 Literature Review

2.1 Radon Gas

2.1.1 What is Radon Gas?

Radon (Rn) is a noble gas formed as a product of radiogenic decay within the uranium-thorium decay series and has a half-life of 3.84 days (Figure 2-1). Radon isotopes undergo alpha decay that give rise to a series of short-lived alpha and beta emitting progeny that produce significant radiation doses (Baskaran, 2016). After its short half-life, it decays to metals polonium, lead, and bismuth. Mapping the concentration of decay products provides utility to trace and quantify radon gas variation, often with enhanced measurement capability over radon gas volumes (Harley, 2017).

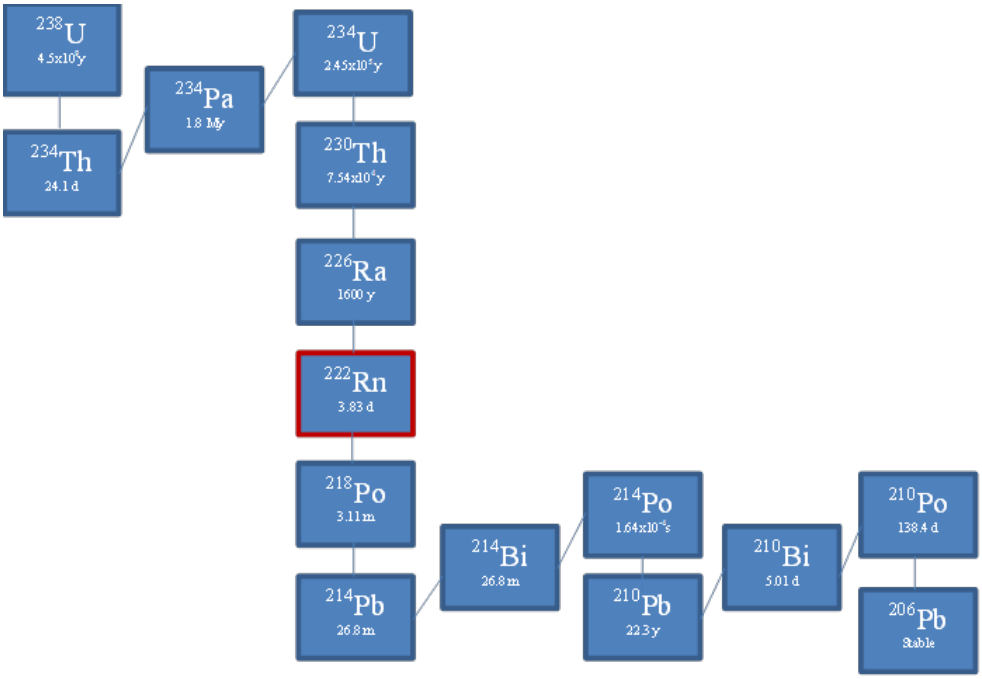

Figure 2-1 Overview of the uranium-thorium decay chain including half-lives. Radon gas (222Rn) has a half-life of 3.83 days and is positioned between Radium (226Ra) and Polonium (218Po).

2.1.2 Radon Surveys in Uranium Exploration

Radon gas detection techniques were developed based on the premise that it is released from geothermal systems and can be detected at or near the surface after it has travelled through the substratum (Malimo, 2012). Many studies of radon gas are driven by the need to quantify radiation doses due to the efflux of radon from soil into the atmosphere (Huxtable *et al.*, 2017). The counting of radon decay products deposited onto collectors is an effective method for delineating radon anomalies in uranium exploration (Card and Bell, 1982).

Uranium mineralization, in an unconformity-type deposit model, forms at the contact between the underlying crystalline-basement and the overlying sandstone cover (Kyser and Cuney, 2008). Broadly speaking, uranium within this model is associated with reactivated faults, which act as a conduit for uranium-bearing fluids. The unconformity contact provides a redox gradient allowing for the precipitation of uranium. Above background values of radon gas occur in measurable amounts at the earth's surface as it migrates through the structural conduit or permeates up through the porous sandstone (Ramola *et al.*, 1989) (Figure 2-2).

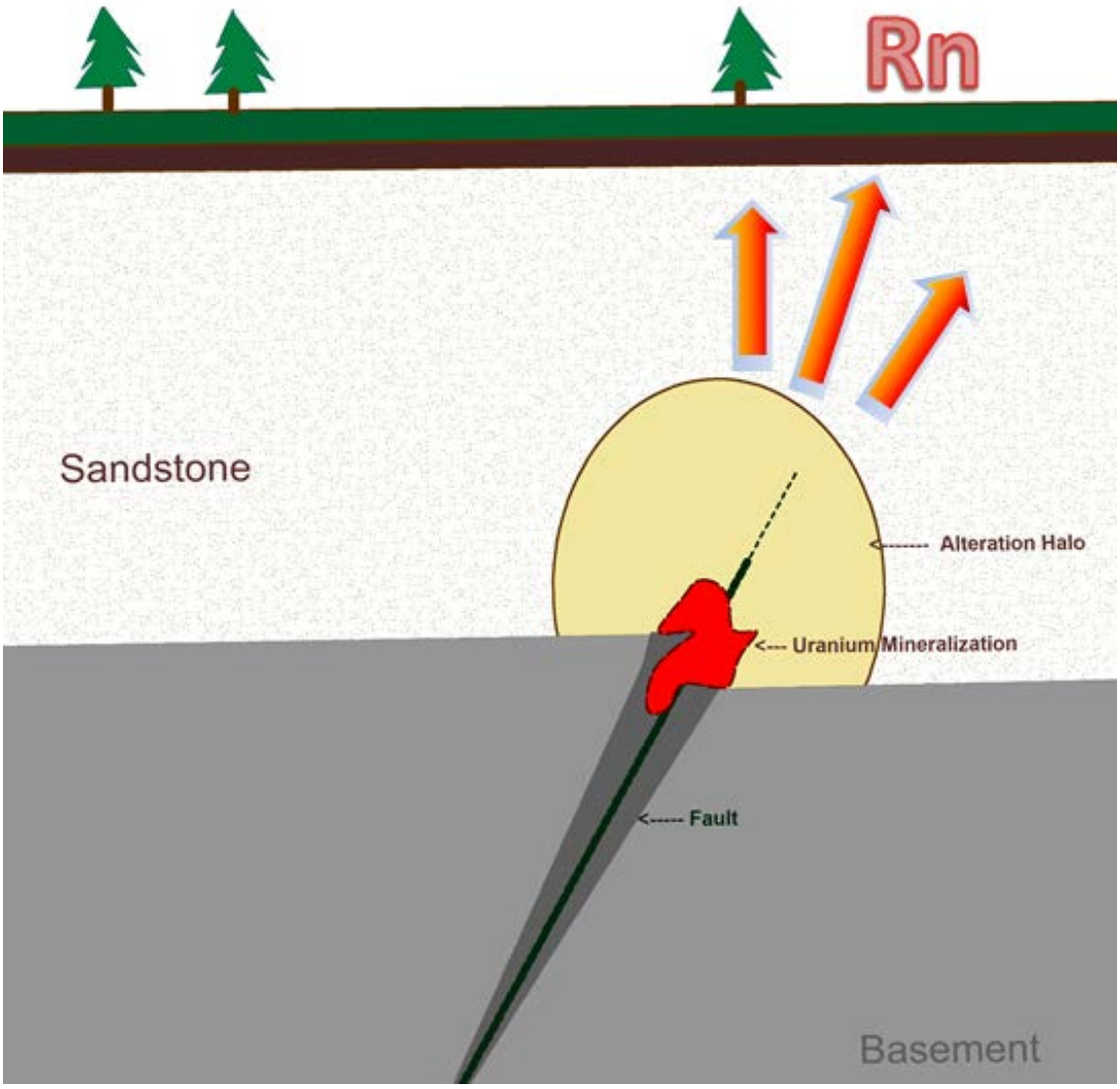

Figure 2-2 Idealized schematic of an unconformity-uranium deposit.

2.1.3 Current Detection Methods

Radon measurement techniques use the physical and nuclear properties of radon, specifically the presence of an alpha particle, for identification (Pacer, 1980). Many techniques for radon detection exist including the ionization chamber method, zinc sulfide detector method, and thermo-luminescence detection method. Radon data acquisition methodologies include the use of rate-meters, digital radon detectors, radon tube sampler method, and track-etch radon surveying. The dominant methods of radon data referred to in this study are the radon tube sampler method,

representative of the historic data set, and Electret Ion Chamber (EIC) method, from a survey performed in 2016. The EIC method uses a passive monitor consisting of a positively charged electret within a chamber placed in the ground for several hours. The negative ionizing effect of the gas causes a flux in charge within the electret and is converted into a flux-measurement of radon concentration (RadonEx, 2015).

2.1.4 Transport Mechanisms and Depth of Resolution

Transport mechanisms of radon include air and water, either on its own or attached to an aerosol (Gurau *et al.,* 2014). Exactly how far radon can travel from its source before its half-life lapses depends on the transport mechanism(s) at play (Baskaran, 2016). If by diffusion alone, it is estimated that it can only travel 10 to 20 meters before its short half-life of 3.8 days lapses; where geothermal induced convection is involved, radon has been reported to travel nearly 100 meters. Gases measured in soils are generally diffusive in nature and are strongly disturbed by environmental factors such as atmospheric pressure, soil moisture, and soil temperature (Pinault & Baubron, 1996).

Radon, which is water soluble, is absorbed by trees and plants through the uptake of groundwater via their root systems and released into the atmosphere by transpiration. One study showed, in a forest comprised of eucalyptus trees spaced four-meters apart, trees may account for up to 37% of the radon that is released from the ground during the middle of the day when transpiration rates are high (Jayarante, 2011). In another study, the movement of radon and radium was described by incorporating vegetation uptake mechanisms into a one-dimensional model in order to determine the feasibility of using vegetation in reclamation processes in contaminated soil. It was concluded that vegetation uptake significantly reduced radon concentration in soil and it ultimately limited the volatile nature of the gas by supporting it in aqueous phase (Kozak *et al*., 2003).

2.1.5 Limitations of Radon Surveys

Limitations of radon surveys for uranium exploration are dominantly attributed to resolution depth. Uranium exploration with target depths greater than 100 meters generally do not use radon surveys as a discovery tool because they are considered outside the travel capacity for the

gas. Additionally, repeatability issues exist when dealing with radon gas measurements due to its diffuse nature as well as variation attributed to temporal variation in atmospheric effects including barometric pressure which influences its mobility, however, the surveys generally work well at identifying broad-scale anomalies.

2.2 Biochemical Surveys and Uranium Exploration

Between 1979 and 1982 biogeochemical surveys were commonly performed for uranium exploration within Northern Saskatchewan's Athabasca Basin (Dunn, 2007). The surveys found uranium to occur in high concentrations in trees above and proximal to known mineralization. The phenomenon was attributed to the upward migration of ions though fault zones; radon track-etch data in the area shows a similar pattern to the biogeochemical survey results (Dunn, 1980). Elevated occurrences of other elements often appeared along with uranium, due to poly-metallic traits of most uranium deposits as well as the transitory nature of elements within the uranium-thorium decay chains.

In the early phases of understanding the biogeochemical surveys, all vegetation species were sampled within the area of interest. Follow-up work, however, often placed a strong focus on only sampling black spruce (*Picea mariana*) because the highest uranium values were obtained from their twigs (Dunn, 1980).

A significant biogeochemical survey of the era, centered roughly on McClean Lake, Saskatchewan, uncovered what is referred to as the "Wollaston Uranium Biogeochemical Anomaly"; the area consists of 10,000 km^2 where all black spruce trees sampled contained what was considered to be anomalous levels of uranium (10 to 1,000 ppm). Within the Wollaston Uranium Biogeochemical Anomaly area, more than twenty uranium deposits have been discovered (Dunn, 2007).

At the time, an attempt was made to understand back-ground levels of uranium in black spruce twigs and needles by performing several traverses near McClean Lake, all of which were not successful. It appears as though the background uranium levels in these zones were over 100 ppm. Interestingly, several black spruce samples from Flin Flon, Manitoba, returned assays with

less than 1 ppm uranium, indicating the significance and amplitude of the Wollaston Uranium Biogeochemical Anomaly and shows that high values of uranium are not indicative of the norm for spruce twigs (Dunn, 1980).

2.3 Remote Sensing of Plant Stress

It has long been understood that changes in leaf pigments, such as chlorophyll and carotenoids, attributed to stress through changing environmental gradients can be detected through spectral reflectance characteristics in vegetation. Vegetation reflectance is governed by properties within the leaf such as internal structure and distribution/concentration of chemical constituents (Barton, 2012). Light is absorbed by pigments such as chlorophyll in the visible spectrum (400–700 nm) and therefore reflectance in these bands is generally quite low. In the near-infrared portion of the spectrum (700–1,300 nm), however, reflectance is higher and largely a function of structural properties of the leaf. The middle infra-red region (1,300–3,000 nm) generally coincides with variation in water and other compounds (Barton, 2012).

By studying differences in the spectral curve between healthy and stressed vegetation, the source of stress can be determined. Vegetation indices are often used, which reduce spectral band combinations to one number, as they aid in mapping changes in vegetation characteristics including stress indicators such as changes in chlorophyll content, physiology, and biomass (Clevers *et al*., 2004).

The region of change in the near infrared reflectance spectrum of vegetation is referred to as the red-edge. Chlorophyll contained in vegetation absorbs most of the light in the visible part of the spectrum but becomes almost transparent at wavelengths greater than 700 nm; resulting in a sharp order-of-magnitude increase in leaf reflectance between roughly 700 and 750 nm (Seager, 2005). Diagnostic characteristics in the spectral curve positioning have been attributed to the source of stress within vegetation. An example is how the position and shape of the red-edge shifts in response to plant stress, either toward shorter wavelengths (blueshift) or longer wavelengths (redshift). Blueshifts were reported in response to heavy metal stress in vegetation (Rock *et al*., 1986, Horler *et al.,* 1983). Radon gas anomalies are considered analogous to areas

with heavy metal stress contamination due to the close relationship between radon gas and its metal progeny.

2.4 Vegetation Indices for Radiogenic Contamination Induced Stress within Vegetation.

Davids and Tyler (2002) performed a study of the effect of radioactive contamination on vegetation in the area of the 1986 Chernobyl Nuclear Power Plant incident and concluded that spectral reflectance measurements can detect stress signatures attributed to the effect of radionuclide contamination within trees, specifically silver birch (*Betula pendula*) and scots pine (*Pinus sylvestris*). Radioactive contamination manifested as changes in leaf pigments and biomass within vegetation in the region. Two indices were highlighted from silver birch showing correlation with elevated γ levels as well as metal contamination linked with 90Sr and 137Cs β-decay radioactive isotopes: chlorophyll red edge and the Three Channel Vegetation Index (TCHVI) (Davids and Tyler, 2002). They concluded that the responses of silver birch and scots pine to radionuclide exposure varied considerably between species. In birch, the effects were expressed via changes in chlorophyll-a concentration within leaves while the influence in pine trees tends to show in the red-edge region and is more complex. Consequently, different spectral responses between vegetation species must be considered when applying optical remote sensing to detect radiogenic contamination (Davids and Tyler, 2002).

2.5 Soil Gases

Radon, in combination with other soil gases, carries information that can be useful in outlining seismic faults and hidden mineral deposits (Pinault & Baubron, 1996). A study performed in Spain effectively used remote sensing techniques to map soil gases, including CO_2 and radon, in tandem with applications in CO_2 leakage detection. Positive correlations were shown between fluctuating radon and CO_2 levels that lead to the conclusion that CO_2 was one of the main carriers of radon gas in the study area. Image analysis showed a correlation between select spectral indices with CO_2 and radon activity, however, results in vegetated areas were not as conclusive at discriminating variation of the gases indirectly through vegetation spectral characteristics (Ortega *et al.*, 2014).

Helium concentration is also of particular interest. Research has shown that mapping radon and helium together is an effective tool to detect and map active fault zones (Walia *et al*., 2005). Radon, compared to helium, is more strongly correlated with uranium and thorium content as well as showing the effects of meteorological influences. When radon is measured on its own, approximately 60% of anomalies appeared to successfully map fault systems. Although radon alone is not strongly correlated to fault positioning, when combined with helium the pattern confirms that mapping the two gasses in tandem provides a powerful tool for mapping seismic faulting activity (Walia *et al.*, 2005).

3 Research Objectives and Hypothesis

The purpose of this research is to explore the potential for mapping of radon gas via spectral changes within vegetation from a satellite platform. The specific objectives are:

1) Mapping the spatial distribution of radon gas within available surface media at Cluff Lake, Saskatchewan.

2) Identify and define the indirect signature of elevated occurrences of radon gas within vegetation communities.

3) Determine if the radon gas signature within vegetation communities can be imaged using satellite based spectral reflectance measurements.

4) Explore the requirements to effectively and accurately map spatial variance of radon gas concentrations using remote sensing techniques.

It is hypothesized that there is a spectral signal linked with radon gas that can be mapped within vegetation communities using optical remote sensing approaches. The indirect signature of radon within vegetation communities is presumably attributed to abiotic stress indicators caused by the radioactive properties of gas, and/or the toxic effects of elevated amounts of its metal progeny.

4 Study Area and Data

4.1 Study Area

The study area is Cluff Lake, Saskatchewan. The Cluff Lake Project, owned by Orano Canada Inc., is a decommissioned uranium mine site and mill complex located in the Athabasca Basin of northern Saskatchewan, approximately 700 kilometers north of Saskatoon and 15 kilometers east of the provincial border with Alberta (Figure 4-1). Uranium exploration activities peaked at Cluff Lake and surrounding area nearly 40 years ago. Vast amounts of work were performed, including extensive radon survey coverage. Radon surveys were responsible for identification of several economic uranium deposits on the property, and some non-economic showings that remain in the ground today. Mining and milling operations commenced in 1980 and were decommissioned in 2002. During Cluff lake's mine life, a total of 64.2 million pounds of uranium (U_3O_8) were extracted from the ground through both open-pit and underground mining techniques (Koning, 2013).

Geologically, Cluff Lake is positioned within the Carswell impact structure (Figure 4-2, detailed geologic map of the Carswell structure is provided in Appendix C). The meteorite impact was determined to have occurred approximately 481 million years ago resulting in a fifty square kilometer circular depression within the Athabasca Basin in northern Saskatchewan (Bleeker *et al.*, 2015). The impact is responsible for a relatively chaotic geologic setting; uranium mineralization is often present as discrete and discontinues pods generally consistent with an unconformity-type deposit model. Several mineralization events have been determined, two uraninite-mineralization events dated at approximately1150 Ma and 1050 Ma; and pitchblende-mineralization events dated at approximately 380 Ma (Bell 1985; Ruhlmann 1985).

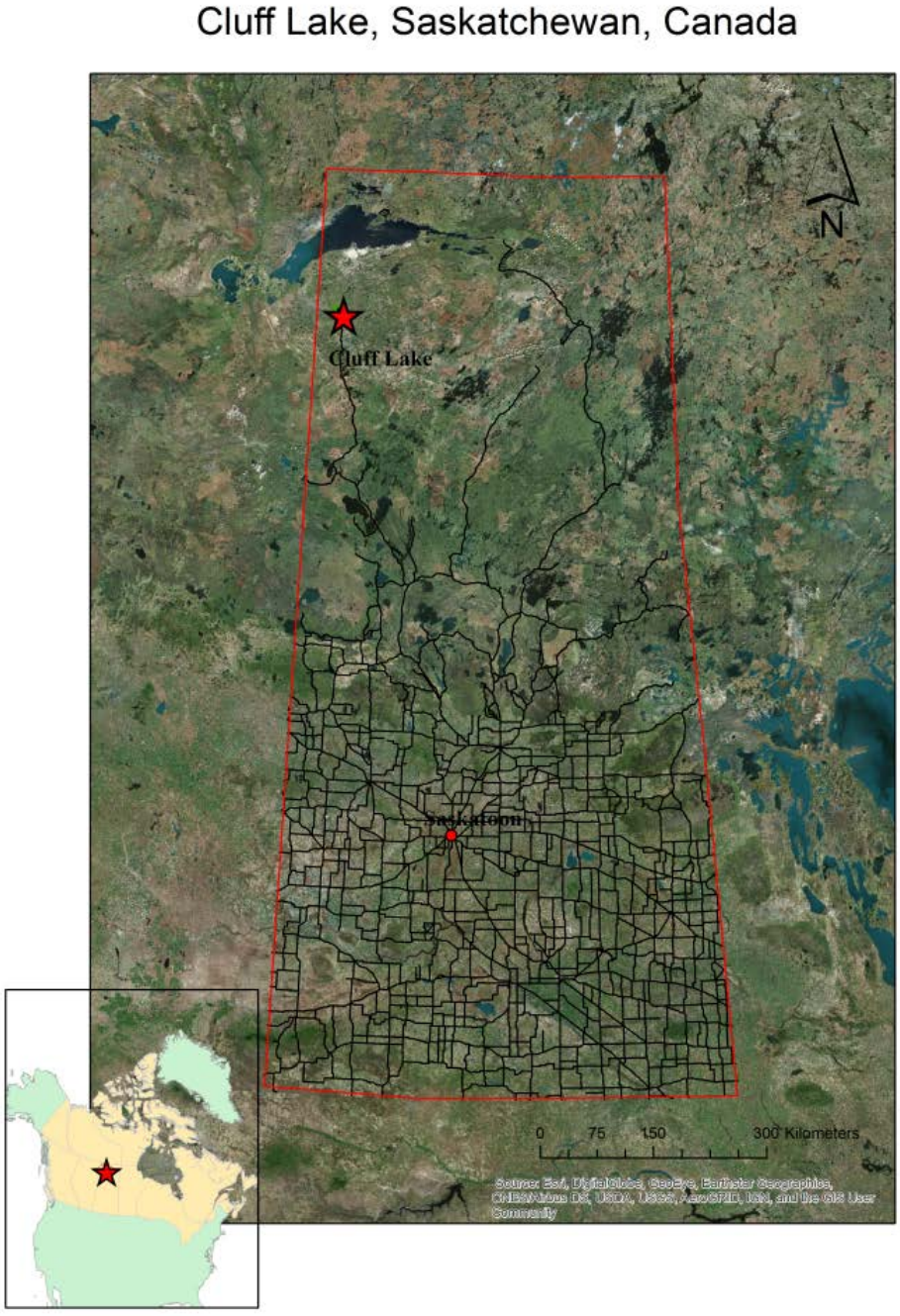

Figure 4-1 Cluff Lake, Saskatchewan; approximately 700 km north-northwest of Saskatoon, Saskatchewan, Canada.

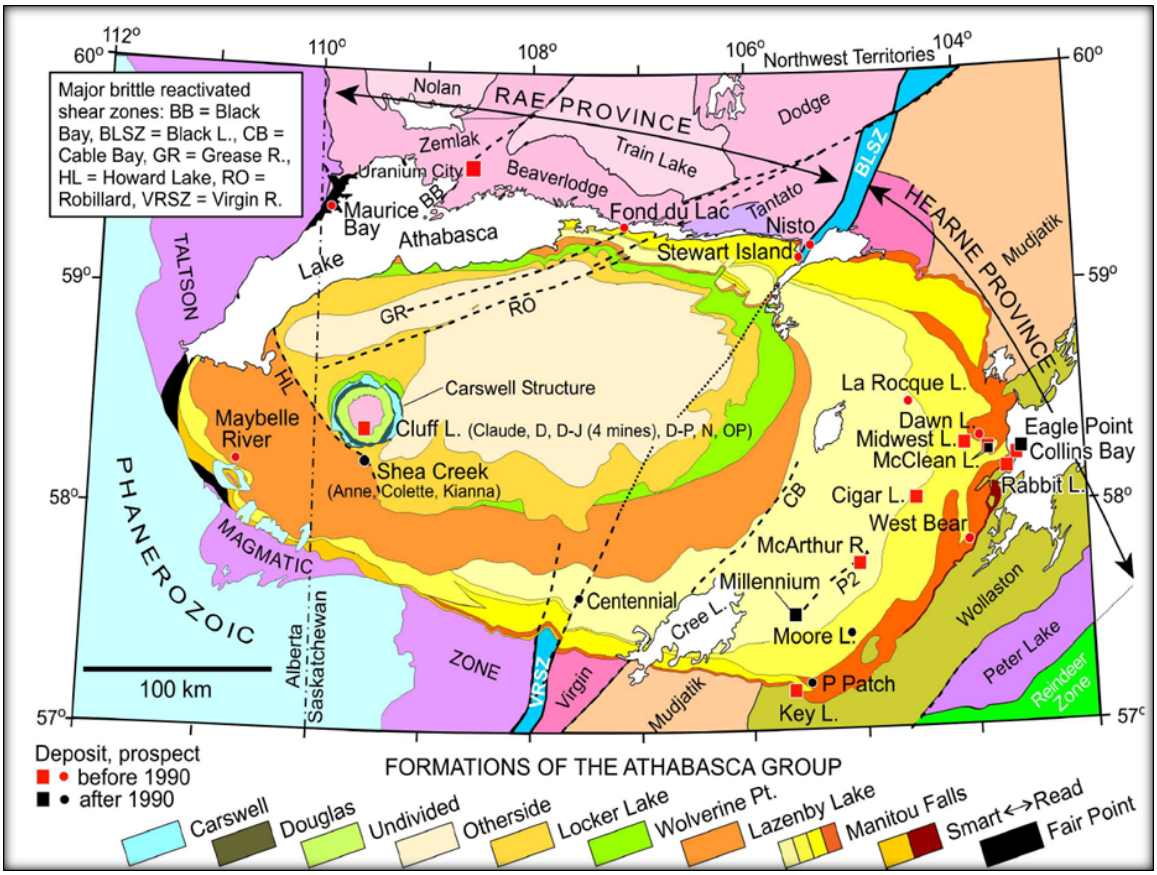

Figure 4-2 Geologic map showing Cluff Lake, Saskatchewan, positioned in the southern portion of the Carswell Structure in the western portion of the Athabasca Basin (Orano, 2018).

4.2 Radon Data

4.2.1 Historic Data

The majority of the radon gas data used in this study was collected by Amok Ltd. between 1978 and 1982 using the radon-tube sampler method (Powell, 1985). Hundreds of surveys were performed, varying in scale and survey method. Generally, the historic surveys were performed at fifty-meter line spacing, with stations every ten meters and results were reported in counts per minute (cmp) (Figure 4-3). At the time, the data were used to generate maps for uranium exploration. Anomalous radon values were used as a vectoring tool for drill targeting; anomalous status was generally given to clusters of radon values above one and a half standard deviations. Approximately 25 square kilometers of historic radon survey data was used in this study (Figure 4-4).

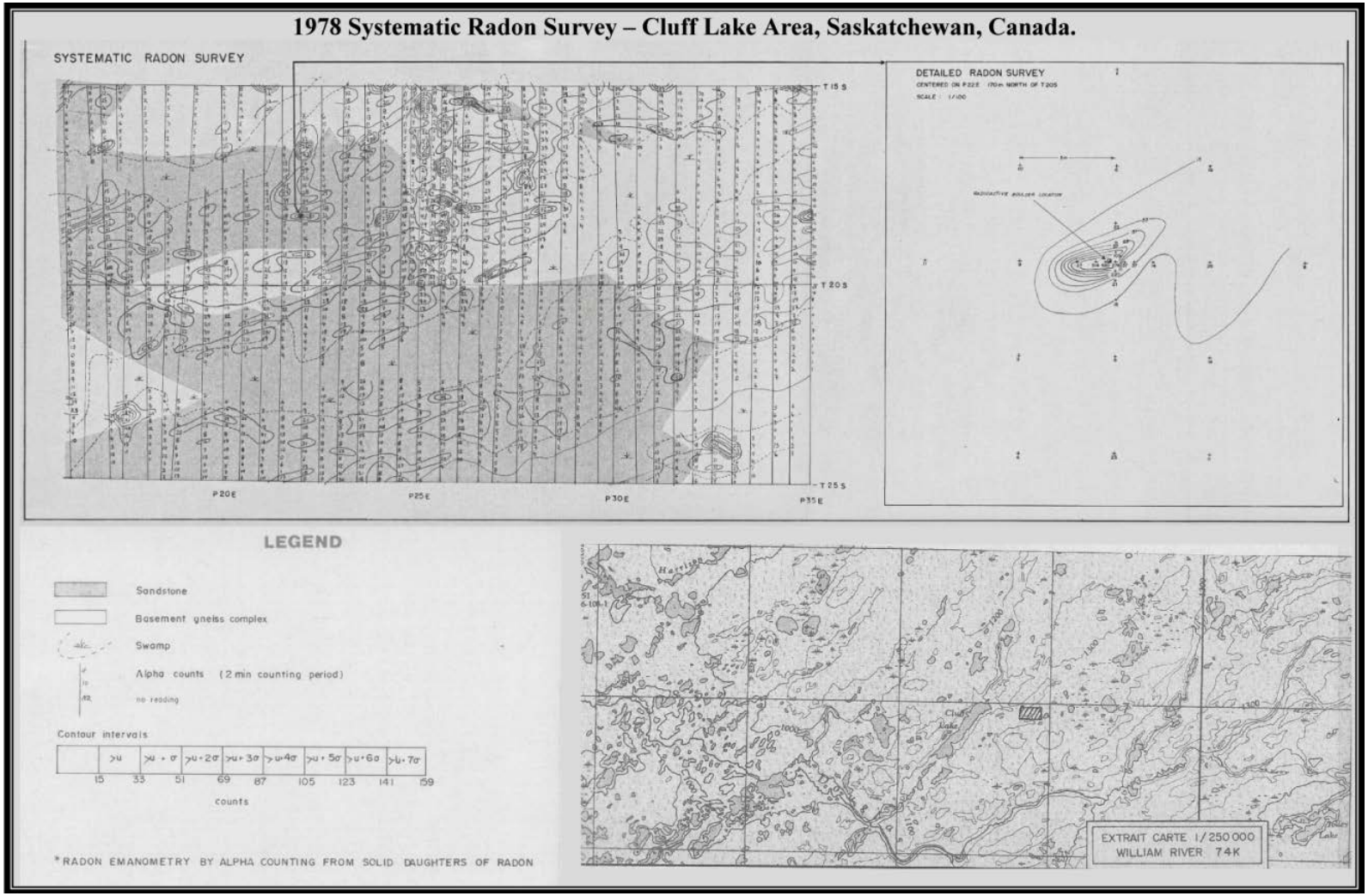

Figure 4-3 An example of a historic radon map on the Cluff Lake property, representative the maps georeferenced and digitized for use in this study. Maps were mostly hand-drawn surveys that varied in scale, survey method, and performed in different seasons and years (Amok, 1978).

4.2.2 Radon Survey – 2016

AREVA Resources Canada (now Orano Canada, Inc.) contracted a radon survey to be performed in June of 2016 on the Cluff Lake property (Figure 4-4). The survey was designed to extend radon survey coverage to previously un-surveyed areas, as well as to validate the extensive historic radon data set by re-sampling a small area. The radon survey consisted of 466 radon-flux readings collected using EIC technology (RadonEx, 2015). Stations were spaced at twenty-five-meter intervals with fifty-meter line spacing.

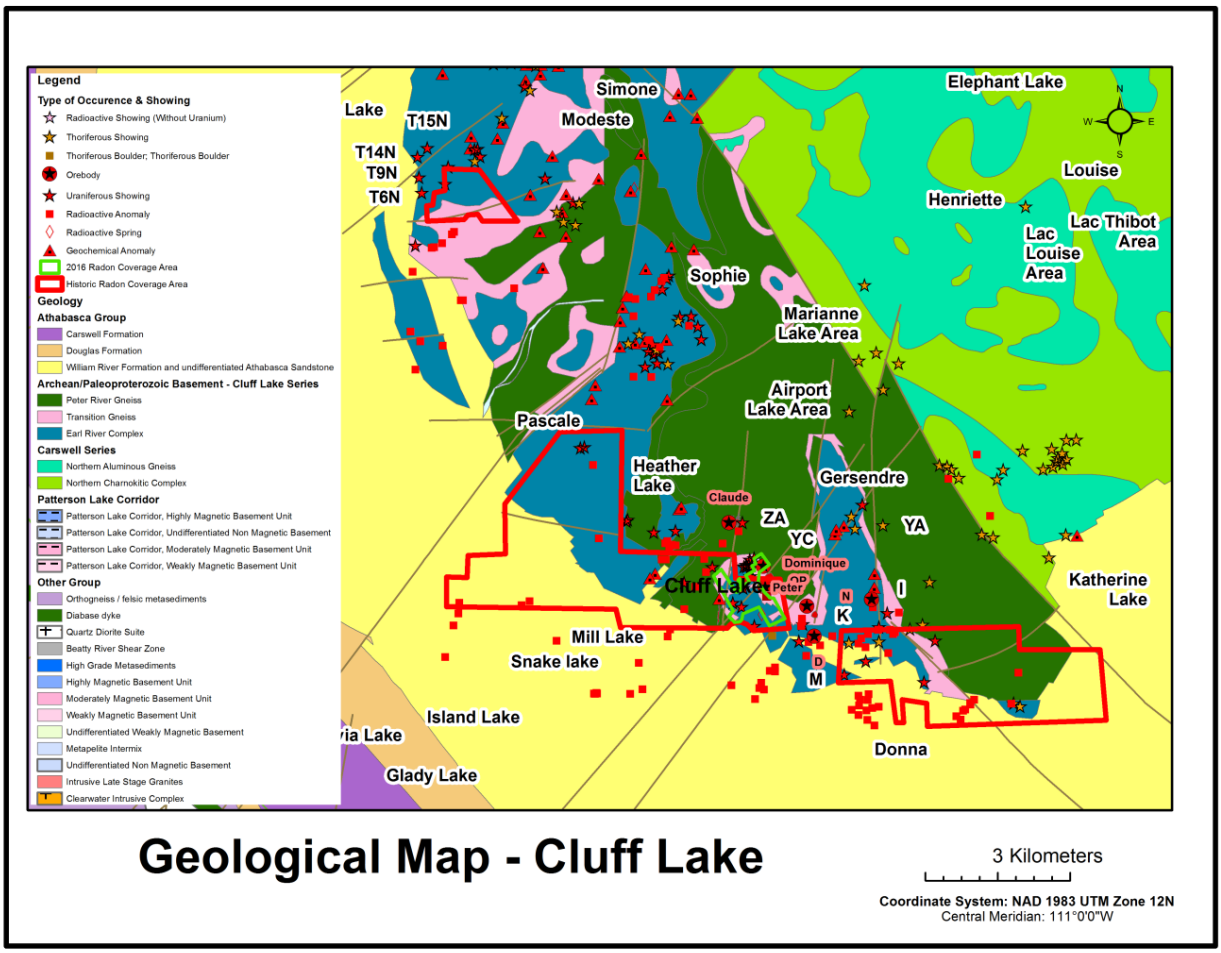

Figure 4-4 Geologic map of Cluff Lake, Saskatchewan, showing area with historic radon coverage (red outline) and the 2016 radon survey area (green outline).

4.3 Additional Surface Media Data

4.3.1 Vegetation Classification

The 1978 vegetation classification map of Cluff Lake and area was produced for pre-mining assessment reports for Cogema Resources (subsequently AREVA Resources, presently Orano Canada Inc;). According to The Cluff Lake Project – CEAA Comprehensive Study for Decommissioning (AREVA, 2001), the map was created based on color infrared aerial photos in combination with ground truthing. A total of 96, 100 m^2 plots were ground surveyed. The mapped vegetation area of focus in this study, due to the presence of overlapping radon survey data, is shown in the red outline northwest of Cluff Lake in Figure 4-5. The area of focus is roughly 12 × 6 square kilometers and covers the ground proximal to what was eventually home to the Cluff Lake mine.

The 1978 vegetation map depicts a vegetation community that is largely comprised of coniferous forest with localized occurrences of deciduous tree cover. Just over half of the vegetation is classified as a jack pine (*Pinus banksiana*) forest mixed with subdominant green alder (*Alnus viridis*). Twelve categories are out-lined in total creating distinctions between combinations of forest vegetation such as jack pine, black spruce (*Picea mariana*), aspen (*Populus tremuloides*) , green alder, white birch (*Betula papyrifera*), dwarf birch (*Betula nana*), and juniper (*Juniperus communis*) as well as non-forest vegetation including lichen, Labrador tea (*Ledum groenlandicum*), willow (*Salix negra*), river alder (*Alnus tenuifolia*), bearberry (*Arctostaphylos uva-ursi*), peat moss (*Sphagnum* spp.), and sedges (*Carex* spp.). Burned areas were also included; however, the original species composition was noted where possible (Table 4.3-1).

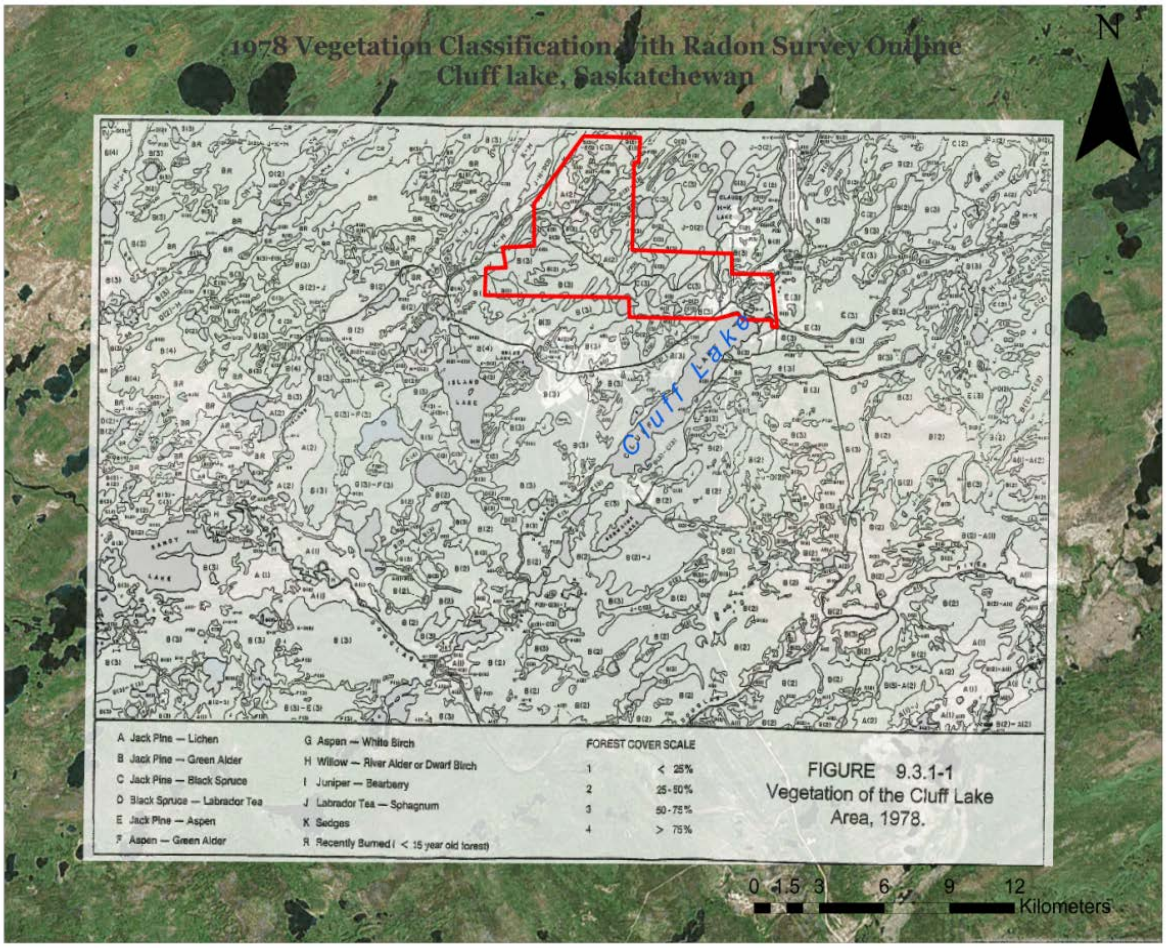

Figure 4-5 Vegetation Classification Map (1978) from Cluff Lake, Saskatchewan. The red-outlined area corresponds to the portion of the map used in this study with overlapping radon data.

Table 4.3-1 Vegetation class details from pre-mining assessment report Cluff Lake, 1978.

Dominant forest species	Sub-dominant forest species	Dominant non-forest species	Ground coverage	Canopy height	Shrubs and ground cover	Observations
A Jack pine Lichen forest type						
Jack Pine		Lichen	75 % (lichen)	5-10 m (Jack pine)	Blueberry, Bearberry, and false heather	coarse soil on summits or upper slopes with southern or southwestern exposure
B Jack pine Green-alder forest type						
Jack Pine	Green Alder		50% (forest species)	15 m (jack pine)	bearberry, blueberry and bog cranberry bunchberry, wild lily of the valley , and twin-flower, moss and lichen	more species diversity than the Jack Pine-Lichen forest type
E The Jack Pine-Trembling Aspen forest type						
Jack pine and trembling aspen	White birch	Bunchberry	50% (forest species)	20 m (forest species)	green alder, blueberry, bog cranberry, bunchberry, mosses, and lichens	moister habitats than other jack pine forests
F Trembling Aspen-Green Alder forest type						
Trembling aspen		Green Alder		20 m (trembling Aspen)	prickly rose, blueberry, bog cranberry and low-bush cranberry, several herb species and mosses were common.	Most species diversity is noted in this category
D Black Spruce-Labrador Tea forest type						
Black spruce			75 % moss/lichen cover	8 m (black spruce)	Leatherleaf, northern laurel, Labrador tea, bog cranberry, moss and lichen	Generally occurred on poorly drained sites with a deep peat layer, usually bordering the Labrador tea/ moss bogs. The black spruce was notably stunted.

4.3.2 Soil Gases

Concurrent with the 2016 radon survey, a soil-gas survey was performed at Cluff Lake consisting of 142 soil gas samples, 16 of which were additionally tested for helium isotopes. Soil gas testing (helium, hydrogen, nitrogen, oxygen, carbon dioxide, methane, ethane, ethene, propane, propene, iso-butane, n-butane, iso-pentane, and n-pentane) was done using custom probes (GCHEM Ltd) and analysis was performed by the André E. Lalonde AMS laboratory at the University of Ottawa.

4.3.3 Soil-type, Till, Saturation, Elevation

Elevation and soil saturation data were obtained from GeoGratis (http://geogratis.gc.ca, 2017); surface geology data including a glacial till map were provided by Orano Resources Canada Inc.

The surface geology map was generated in 1971 according to surface mapping in combination with aerial photograph consultation.

4.4 Satellite Data

4.4.1 Sentinel-2A

Sentinel-2A was chosen for this study because it is one of the few satellite data sets available to the public that has red-edge imaging capabilities. It is a multispectral instrument that collects images in the visible and infrared portions of the electromagnetic spectrum and records in thirteen spectral bands with spatial resolution varying between 10 and 60 meters (Figure 4-6). The images used in this study have 20 meter resolution. The Sentinel-2A data were downloaded from Copernicus Services Data Hub; images were collected on June 6th, 2017.

4.4.2 Worldview 2

Worldview-2 data were supplied by the DigitalGlobe Foundation. The satellite includes a panchromatic sensor with a 46 cm maximum resolution and a multispectral sensor of 184 cm; the image was collected on April 3rd, 2017. Data are collected in eight bands, including one in the red-edge region (Figure 4-6).

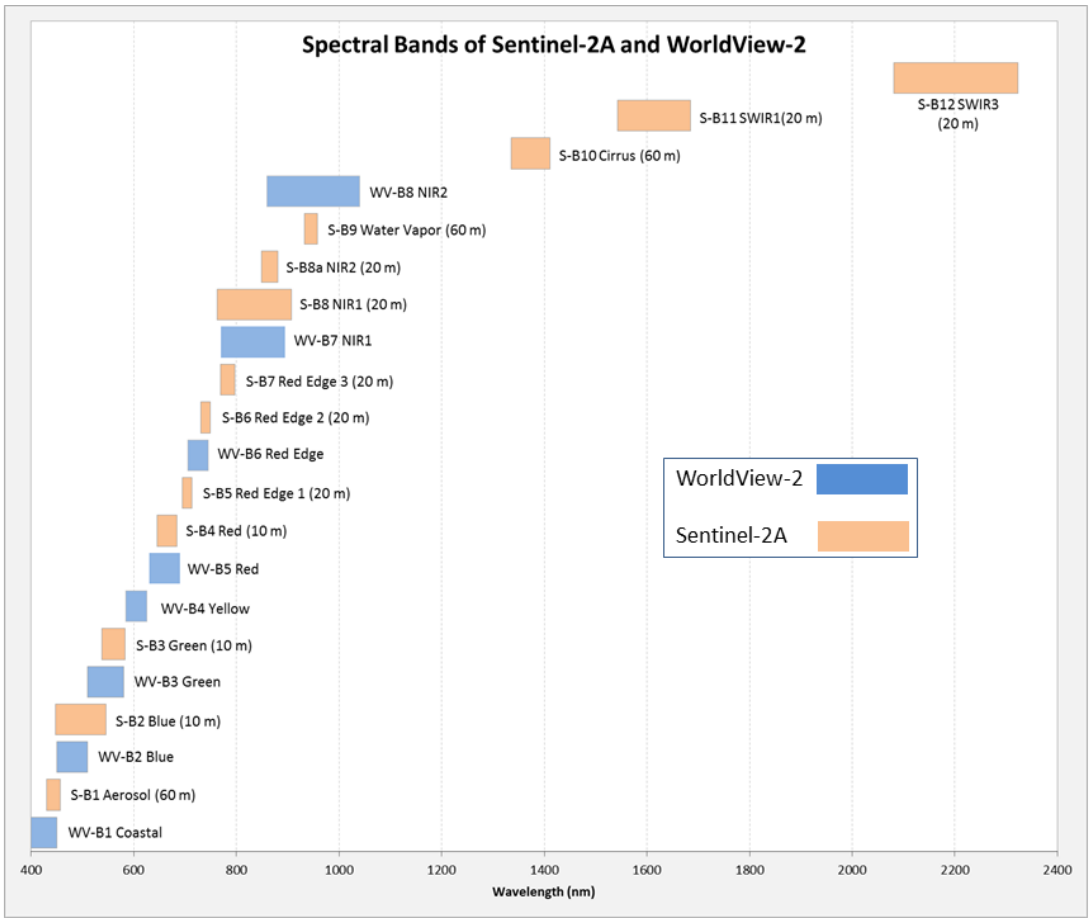

Figure 4-6. Spectral bands of Sentinel-2A and Worldview-2 satellites.

5 Methods

The methodology approach was divided into two main segments. The first focuses on data collection, digitization, preprocessing, and validation for radon and all available surface media data. These intensive steps formed the foundation for the second stage of work which focuses mainly on remote sensing techniques (Figure 5-1).

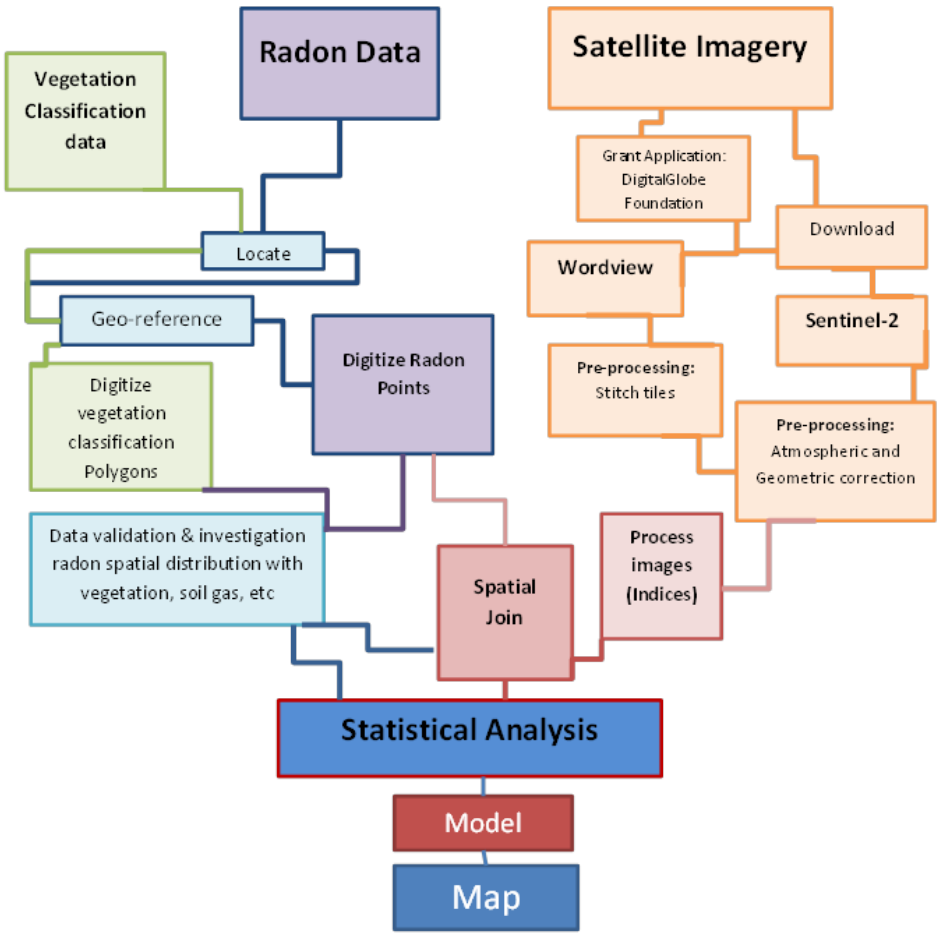

Figure 5-1 Methodology flow chart.

5.1 Data Collection, Geo-referencing, and Digitizing

5.1.1 Radon Data

The bulk of the radon data from Cluff Lake had been archived and sent to storage after the mine was decommissioned. At first, it was unknown exactly where all of the maps were located and how many radon survey maps existed. It is now estimated that over 50 km^2 of coverage exists on the property.

Once the historic radon maps were located, they were georeferenced and the radon point data were digitized using ArcMap 10.5. The historic maps are of variable quality as the majority of them are hand drawn. In many cases, clear coordinates were not displayed; therefore, geo-referencing largely relied on the location of lakes and development of a master-map connecting historic grid-lines. A significant amount of pre-processing work was required to get the legacy radon data into the digital format that was used in this study.

5.1.2 Vegetation Classification

The 1978 vegetation classification map was georeferenced using lakes and streams in the area. The coordinate system was not recorded on the map but it was georeferenced using UTM NAD 27 Zone 12, as that is the dominant coordinate system quoted in reports from the same era.

5.2 Validation of Historic Radon Data Set

The sample methodology and survey parameters for the historic radon survey and the survey performed in 2016 are different, and therefore are difficult to compare directly. In an attempt to do so, a 12.5-meter buffer around each of the 2016 sample station locations was created. Historic radon points that fell within the buffer zone were spatially joined to the 2016 sample locations. A mean value was then calculated for the historic radon (generally two to ten historic values were joined to one 2016 survey value). The two data sets consist of the mean historic radon cpm (proximal to 2016 stations) and 2016 radon survey values, where overlap exists. Both data sets were standardized to have a mean of zero and standard deviation of one. Areas of “disturbed ground” comprise approximately 25% of the 2016 survey. These variably contaminated samples

were removed from further analysis and the remaining 275 joined relatively un-contaminated values were then plotted, using absolute values and kriged grids, for comparison.

5.3 Investigation of Spatial Distribution of Radon Gas

The historic radon data set was spatially joined with available surface media data including: vegetation classes from 1978, soil type, soil saturation, and elevation. In some cases, especially the vegetation classification, comparison was made by using descriptive statistics, including mean and standard deviation of radon within each nominal vegetation class. Where the data sets were both numeric, correlation analysis was used to interpret relationships using SPSS software (V25.0).

Spatial and correlation analysis between various soil gases and radon data were performed using ArcMap 10.5 and SPSS (V25.0) software, respectively. The analysis only used the 2016 survey data which was performed in a small area north of Cluff Lake proper.

5.4 Image Pre-processing and Data Extraction – Sentinel 2A

Geometric and atmospheric corrections on the Sentinel-2A satellite data using PCI Geomatica 2017 software were completed. The absolute reflectance digital values were extracted from the image and was the base for further analysis; a true color Sentinel-2A image is shown in Appendix A.

Once pre-processing was complete, the digitized radon data set and corrected satellite image(s) were imported to ArcMap 10.5 to begin analysis, both visual and statistical. A buffer with a five-meter radius was created for each radon X,Y coordinate and a spatial join was performed with Sentinel-2A data. The Sentinel-2A band data and each corresponding radon point values were exported for statistical analysis using Microsoft Excel (2010), SPSS (V25.0), and R statistical software(V3.3.1).

5.5 Image Pre-Processing and Data Extraction – WorldView-2

The Worldview-2 data required extensive pre-processing including geometric and atmospheric corrections using PCI Geomatica (2017) software and the stitching together of tiles. Upon acquiring the data, it was planned to perform a similar sequence of statistical analysis as was performed with the Sentinel data. Since the spatial resolution of the imagery was much higher than the ground survey data this was not feasible (1 meter compared to approximately 25 meters). The high-resolution WorldView data was primarily used to aid in visual validation of the radon pseudo-survey maps generated in the final stages of this research using Sentinel-2A images.

5.6 Statistics and Trend Detection

5.6.1 Spectral Characteristics

The historic radon data set is robust, with approximately 42,000 data points, and heavily skewed. The majority of the points lie in what is considered to be the background range for radon values, with only a small population of what is considered to be moderate to anomalously high. Correlation analysis was initially performed with the entire data set using the individual radon point value and the extracted corresponding spectral band values. This failed to highlight meaningful relationships due to the size and distribution of the data. A natural-logarithmic transformation was applied to the radon data-set to better approximate a normal distribution. To reduce the data set, it was subsequently grouped into six categories based on one increment of standard deviation (σ). Three groups both above and below the mean (μ) were generated as follows: Goup 1(<-2σ), Group 2 (-2σ→-σ), Group 3 (-σ→μ), Group 4 (μ→ σ), Group 5 (σ→2σ), and Group 6 (>2σ). The means of each of the spectral bands corresponding to the radon-grouped data were calculated and plotted to observe the differences in character therein.

5.6.2 Vegetation Indices

A heuristic approach was taken with selection of vegetation indices with a strong focus on those including the red-edge and NIR band(s). Most of the vegetation indices discussed in this study were found in the Index Database (IDB) specifically for Sentinel-2 data (https://custom-

scripts.sentinel-hub.com, 2018) (Table 5.6-1). Two vegetation indices, the RnVI(1) and RnVI(2), are proposed as a product of this research. They were generated by modifying the TCHVI index using Sentinel-2A bands in order to maximize the observed differences in spectral curve between background, moderate, and high values of the gas (Table 5.6-2). Vegetation index values using sentinel-2A spectral bands were generated for each of the logarithmically grouped radon data points and subsequent analysis of variance was performed. Correlation and regression analysis were performed using SPSS software (V 25.0).

Table 5.6-1 Referenced Vegetation Indices (Sentinel 2A bands).

Abbreviation	Name	Formula	Source
CIrededge	Chlorophyll Index Red Edge	$\frac{NIR(2)}{RE(1)} - 1$	IDB
CVI	Chlorophyll Vegetation Index	$NIR(2)\frac{RE(1)}{Green^2}$	IDB
REIPI	Red Edge Inflection Point 1	$700 + 40\left(\frac{\frac{Red + RE(3)}{2} - RE(1)}{RE(2) - RE(1)}\right)$	Herrmann *et al.*, 2011
TCHVI	Three Channel Vegetation Index	$\frac{(Red - Green) - (NIR(1) - Red)}{\lvert Red - Green\rvert + \lvert NIR(1) - Red\rvert}$	Davids *et al.*, 2002; from Yefremenko, 1998

Table 5.6-2 Proposed Vegetation Indices (Sentinel 2A bands).

Abbreviation	Name	Formula
RnVI(1)	Radon Vegetation Index(1)	$\frac{(RE(2) - Red) - (NIR(1) - RE(2))}{\lvert RE(2) - Red\rvert + \lvert NIR(1) - RE(2)\rvert}$
RnVI(2)	Radon Vegetation Index (2)	$\frac{(Red - Green) - (RE(2) - Red)}{\lvert Red - Green\rvert - \lvert RE(2) - Red\rvert}$

5.7 Radon Pseudo Survey Map Generation

The vegetation indices that showed the greatest potential for differentiating between background, moderate, and high levels of radon was applied to the sentinel-2A image using PCI Geomatics (2017) EASI Modeler. The modelled image channel was exported from PCI geomatics and imported into ArcMap. All data points outside of the moderate and high range of radon gas values were masked and a color contour radon pseudo-survey map was generated.

6 Results

6.1 Digital Compilation of Historic Radon Data

The compiled legacy radon data set consists of 42,055 radon data points. Compilation of the data allowed for a more regional scale evaluation of the data as well as formed the basis for progressing with this study. Descriptive statistics for the radon data are shown below (Figure 6-1).

One of the main sigmoidal shaped radon anomalies coincides with the Janine area and is one of the key areas of focus moving forward (Figure 6-1). Known uranium mineralization remains in the ground at Janine today. Geologically, the Janine area is positioned within the Paleoproterozoic Peter River Gneiss series (Figure 4-4). Uranium mineralization is characterized as a series of shallow discontinuous pods of uranium. Initially, it was thought that due to the shallow nature and positioning of the uranium, the primary deposition was related to glacial events, however, after further investigation, the shallow pods showed a deep root system and the initial hypothesis was abandoned (Powell, 1985).

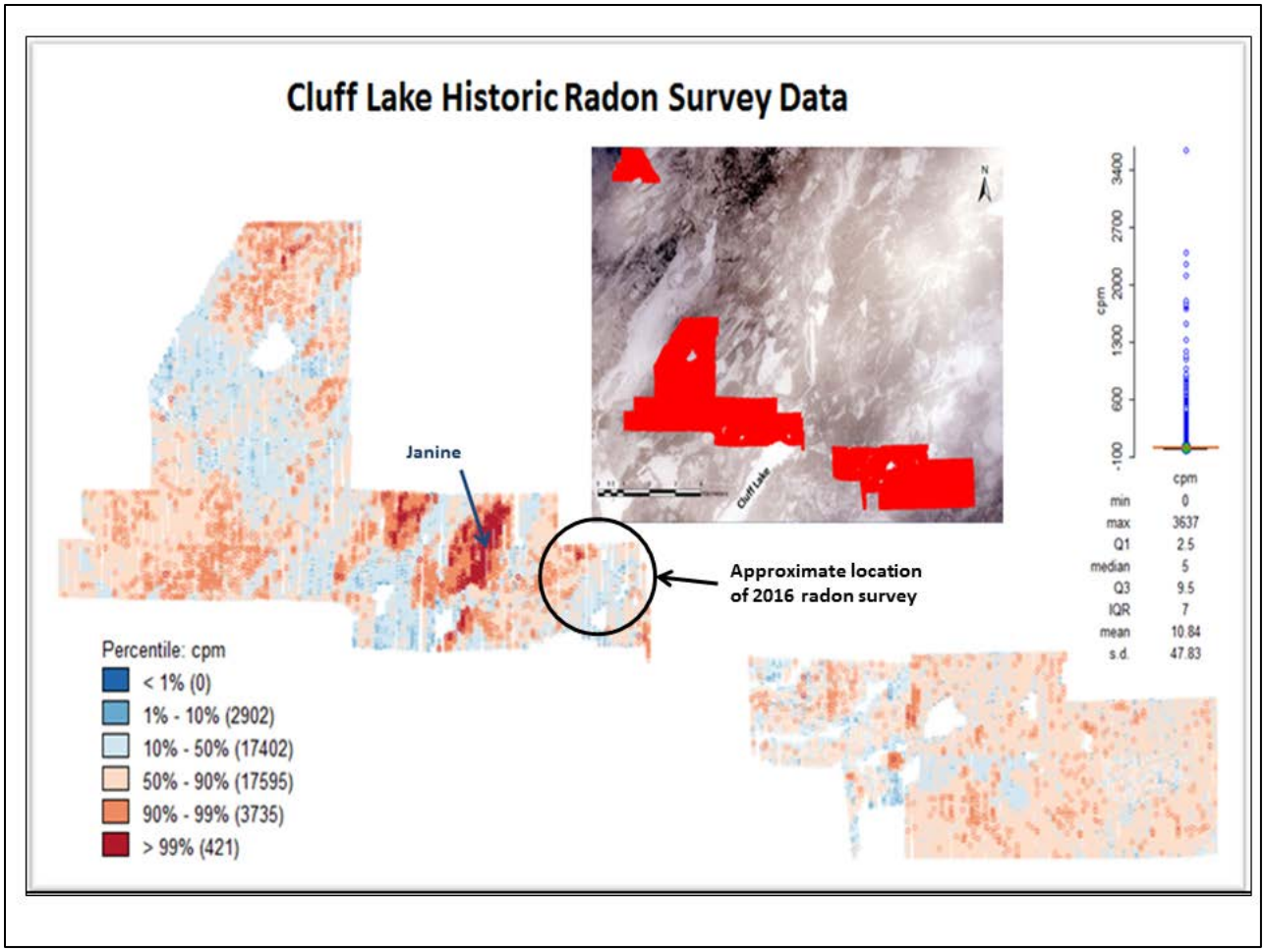

Figure 6-1 Percentile-map and descriptive statistics of digitized radon data from the Cluff Lake project (n=42,055).

6.2 Validation of Historic Radon Data Set

In order to understand the repeatability and accuracy of the large historic radon data set, a small survey was designed in 2016 which provided partial overlap on historic grids. One of the main differences is that the modern survey highlights contamination in the area due to mining infrastructure that would not have been present at the time the radon data was collected during the exploration phase at Cluff Lake (Figure 6-2 A&B).

A **B**

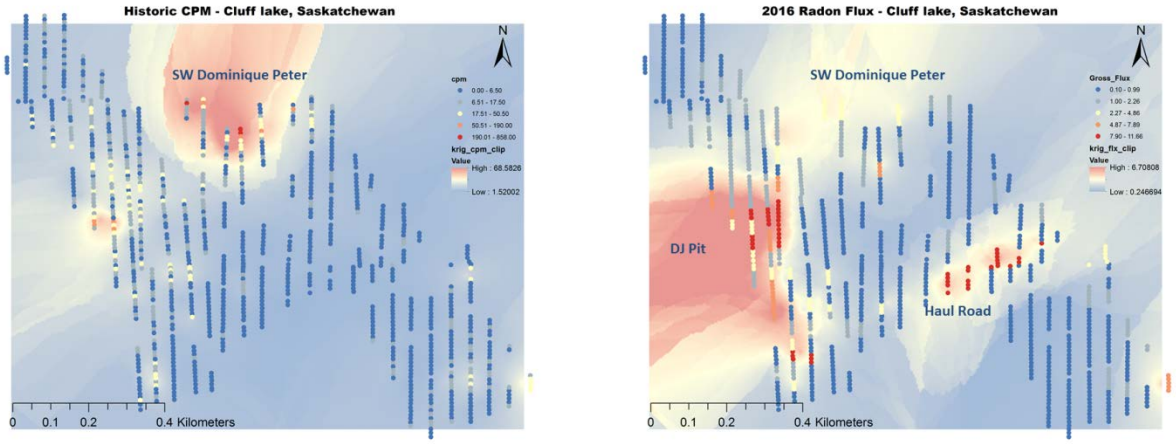

Figure 6-2 A) Historic radon values (cpm) spatially joined with 2016 radon survey data. Kriging highlights several local anomalies; the most significant feature is to the North (SW Domonique Peter). Figure 8 B) 2016 radon flux values spatially joined to historic data. Kriging highlights contaminated areas (haul road and DJ pit) but also shows a feature to the north coincident with known mineralization at SW Domonique Peter.

The 2016 survey data were plotted with the contaminated points removed to further compare the two surveys. The line chart shows a clear relationship between data sets (Figure 6-3). Generally, the historic radon peaks are more subdued due to the effects of averaging multiple values for one point. All samples that were noted as disturbed in the 2016 survey were removed for consistency. Contaminated points in the Kriging map are focused on the haul road and other mining infrastructure. The 2016 radon flux data is overall slightly noisier than the historic data which may be attributed to minor local contamination and/or the averaging of the historic data. Overall, a reasonable correlation between the historic radon data set and 2016 survey data was observed.

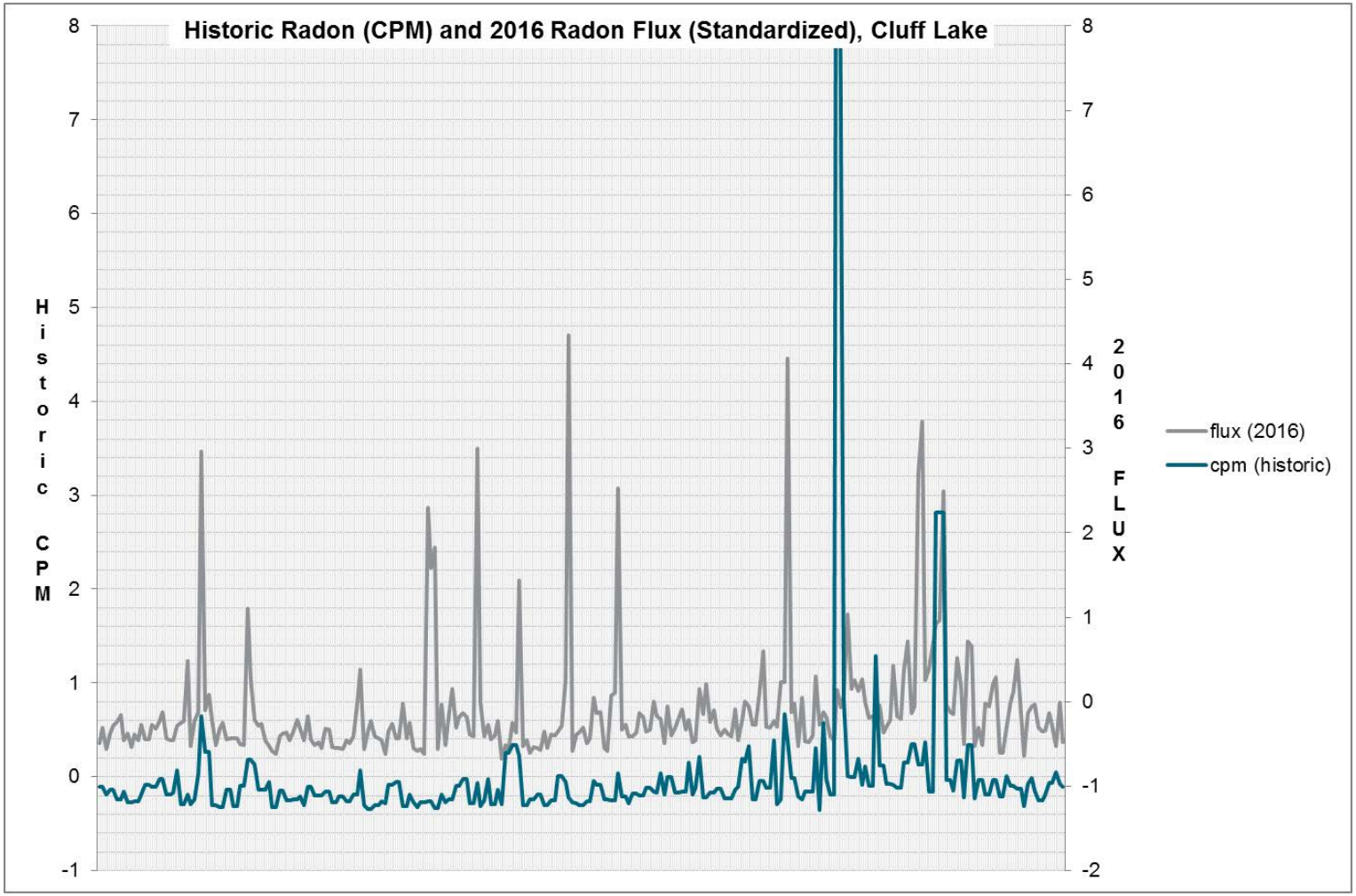

Figure 6-3 Spatially joined 2016 and historic radon data with 2016 samples taken (disturbed/contaminated samples removed).

6.3 Spatial Distribution of Radon Gas

Statistical and visual correlation analysis was performed between radon gas and all available surface media at Cluff Lake in order to understand the spatial variation of radon depending on its co-distribution with other environmental variables.

6.3.1 Soil Gas

Graduated symbol plots were generated for radon, carbon dioxide, and helium (Figure 6-4**),** some descriptive statistics for the data sets are shown below (Table 6.4-1). In this area, the anomalous radon values highlight a northeast trending feature coincident with known weakly mineralized faults in the area. A similar visual trend exists between radon gas values and carbon dioxide, and to some extent, helium. As discussed previously, elevated radon is highlighting some of the mining infrastructure, specifically the east-northeast trending haul road in the southern portion of the radon survey.

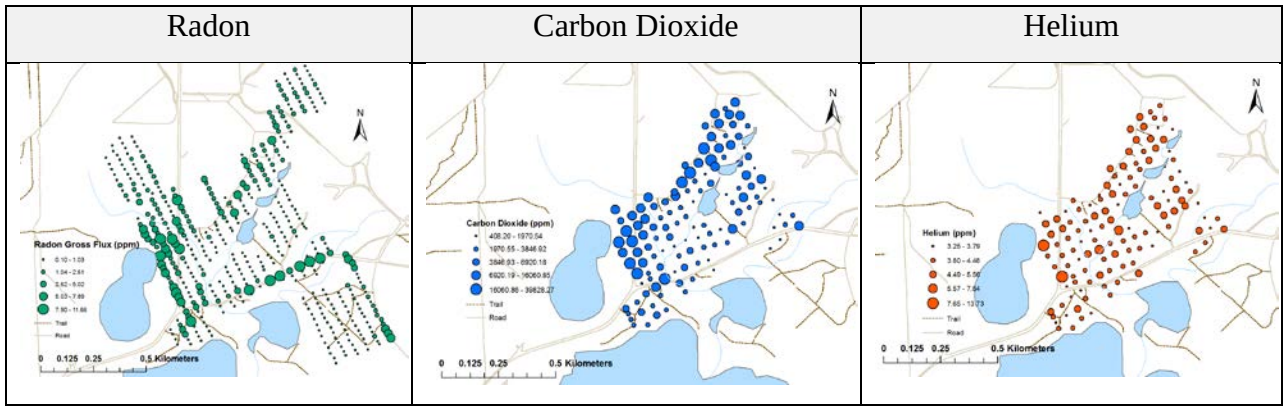

Figure 6-4 Graduated symbol plots for Radon, Carbon Dioxide, and Helium show a similar northeast trend.

Table 6.4-1 Descriptive statistics for Rn, He, and CO_2 gases (2016)

	Rn (pCi/m2/sec)	He (ppm)	CO_2 (ppm)
Minimum	0	0	0
Maximum	11.66	13.73	3.98e+004
Mean	1.47	0.03	46.48
Standard Deviation	2.00	0.40	780.50
N	466	142	142

According to correlation analysis results between radon and various soil gas values (Table 6.4-2), a strong positive relationship is observed with γ (radiometry) values and radon gas. This is not surprising due to the radioactive nature of the gas. The correlation co-efficient for carbon dioxide shows a weak positive relationship (r=0.360). Helium, another soil gas of potential interest due to its relationship with radon and seismic events, shows a very weak positive linear relationship with radon (r=0.25).

Table 6.4-2 Pearson's correlation coefficients between radon gas (pCi/m2/sec) and: elevation (m), radiometry (γ), helium (ppm), hydrogen(ppm), nitrogen(ppm), oxygen(ppm), carbon dioxide(ppm), and methane(ppm). (N=123)

	r	sig.		r	sig.
Elevation	0.19	0.04*	**N**	0.04	0.68
γ	0.73**	0.00	**O**	-0.07	0.43
He	0.25**	0.01	**CO_2**	0.36**	0.00
H	-0.06	0.51	**CH_4**	-0.04	0.63

*Correlation is significant at the 0.05 level (2-tailed). ** Correlation is significant at the 0.01 level (2-tailed).

6.3.2 Vegetation, Elevation and Soil Type

Soil/till type and topography are potentially critical factors for vegetation community dynamics as they determine factors such as available nutrients, moisture, slope, and exposure to light. The

glacial till map, specifically in areas with radon survey coverage, indicated a relatively homogenous glacial till profile with zones of fluted, grooved, and fluvial eroded moraine (Figure 6-5) (Amok, 1978). As expected, there are more occurrences of moss and sedges in areas that have saturated soil however there is no apparent relationship between these variables and radon gas occurrences at Cluff Lake (Figure 6-6). Correlation analysis was performed between radon values and elevation with only a very weak positive linear correlation observed (r=0.19) (Table 6.4-2).

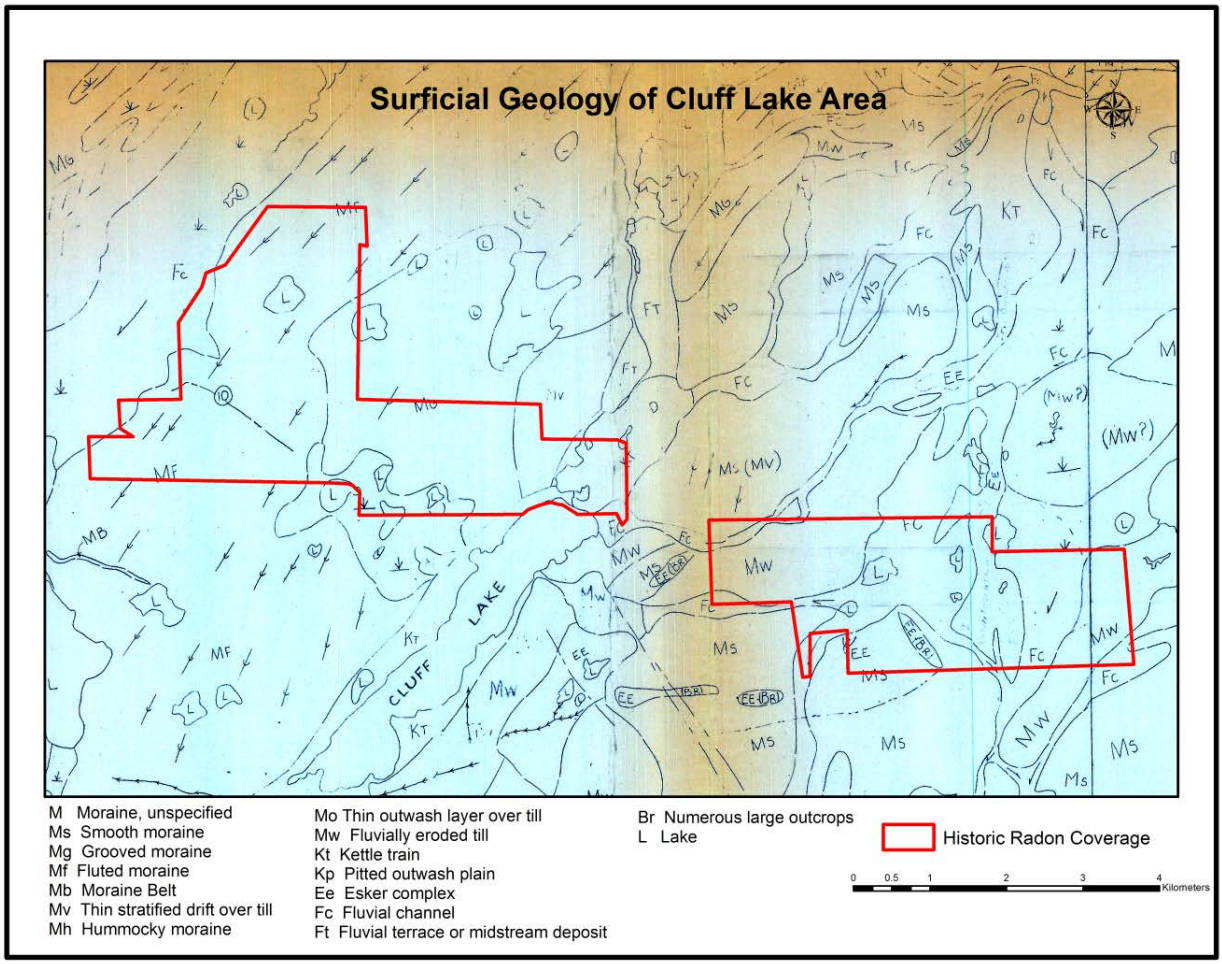

Figure 6-5 Surface geology map of Cluff lake Saskatchewan (Amok, 1978).

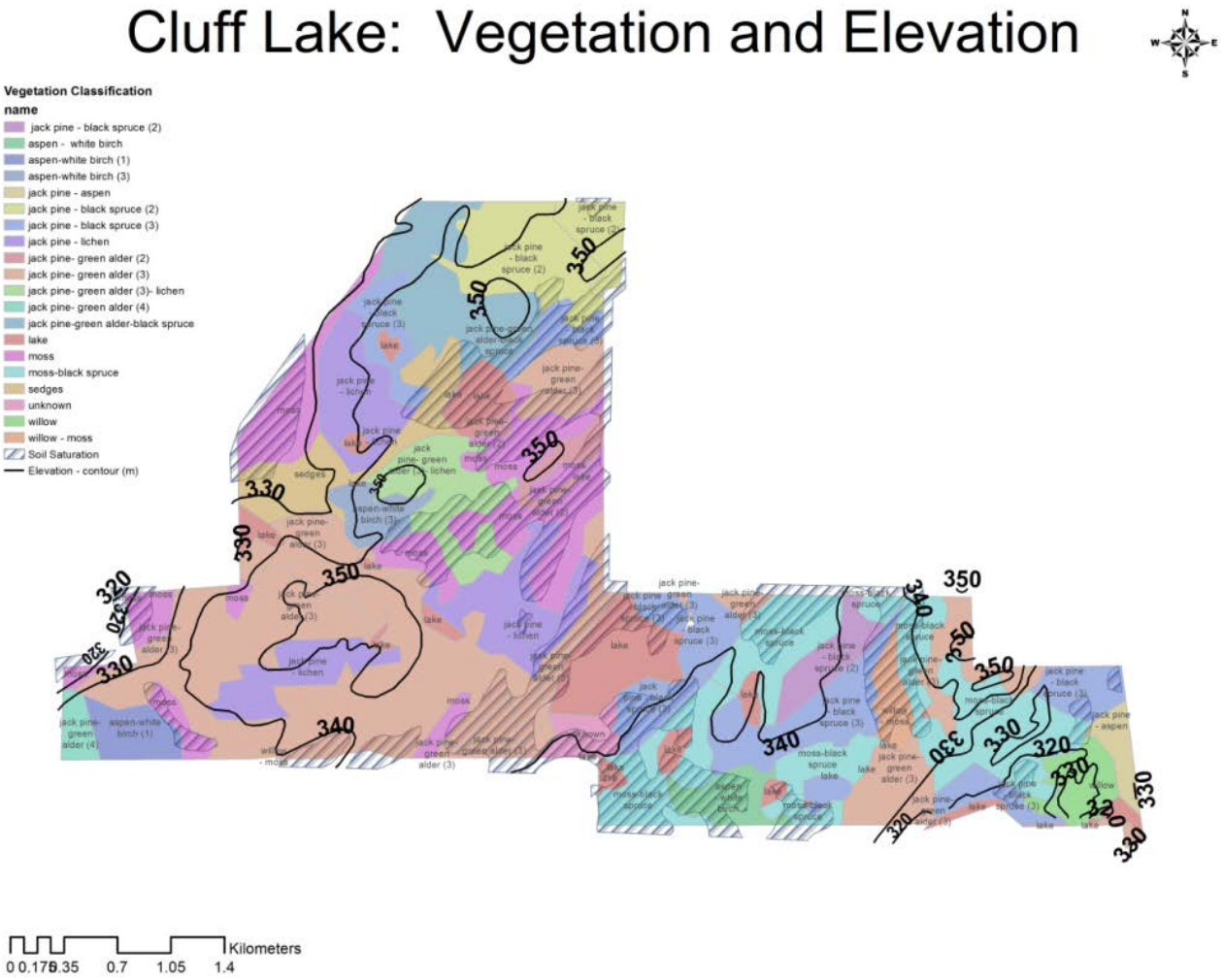

Figure 6-6 Vegetation community map with soil saturation (hatched areas) and elevation contours added.

There was an expected dependence on elevation and vegetation class that was not apparent, at least at the scale of observation on this study. Black spruce, for instance, are generally expected to occur in low laying wet lands (Hogan, 2008), however, by comparison with elevation and soil saturation data, it does not appear that the black spruce varies spatially according to topography in the study area.

Once the radon data and vegetation data sets were digitized, a spatial join was performed using ArcMap. Each radon point was further categorized by the corresponding vegetation class

polygon. There is an observable and unexpected relationship between black spruce occurrence and elevated radon values (Figure 6-7). The plot shows the majority of anomalous radon values occur within communities containing black spruce. In fact, the mean radon value for vegetation polygons that contain black spruce is nearly 50 cpm while for polygons that do not contain black spruce it is zero (n = 24,630). Further correlation analysis was limited by the nominal nature of the vegetation data set and is an area where further research is needed.

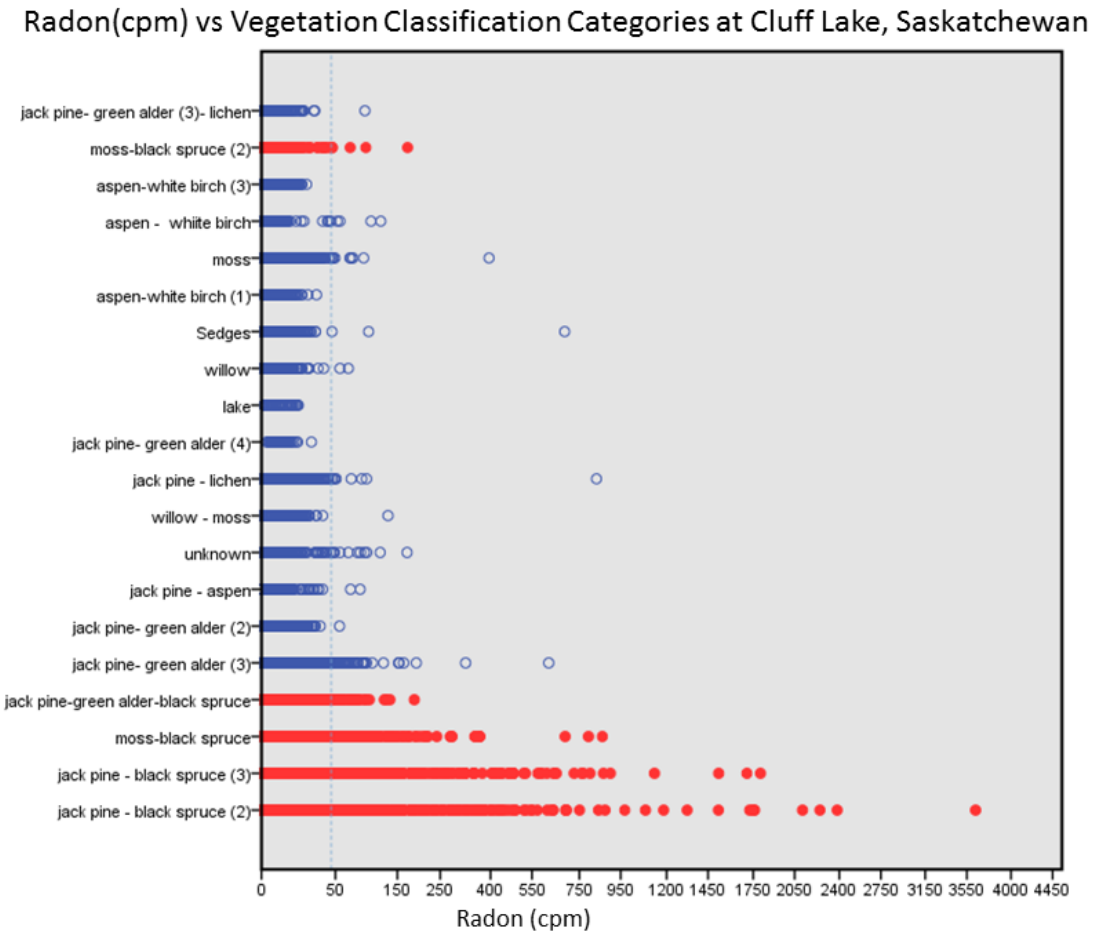

Figure 6-7 Joined radon values within their respective vegetation classes. Red points show radon values in black spruce communities. Blue points are radon values in non-black spruce communities. The dashed line is one standard deviation in the radon data set. The number beside the vegetation class refers to density of vegetation cover (higher number, greater density).

6.4 Spectral Characteristics of Grouped Radon Data

Once the logarithmic values of the radon data set were grouped based on increments of standard deviation, the average value for each of the Sentinal-2A bands was calculated and the spectral curve for each group was plotted (Figure 6-8). The results show a clear variation of reflectance between some groups. The predominant difference is observed in the red-edge to near-infrared regions (700–1400 nm). Groups one through four represent what is considered to be background values of radon gas, with values less than one σ above the mean for the radon dataset. The background groups have a similar trend and show the highest reflectance of all groups. Group five represents moderate radon values between one and two σ above the mean. This group shows an intermediate near-infrared spectral curve positioned between groups representing background and statistically elevated radon values. The highest occurrences of radon gas, represented in group six, shows a stark decrease in reflectance relative to the other groups. Within the visible-light portion of the spectrum (400–700 nm), differences between the average reflectance of radon groups are subtle, yet groups four, five, and six again have the lowest reflectance in this range.

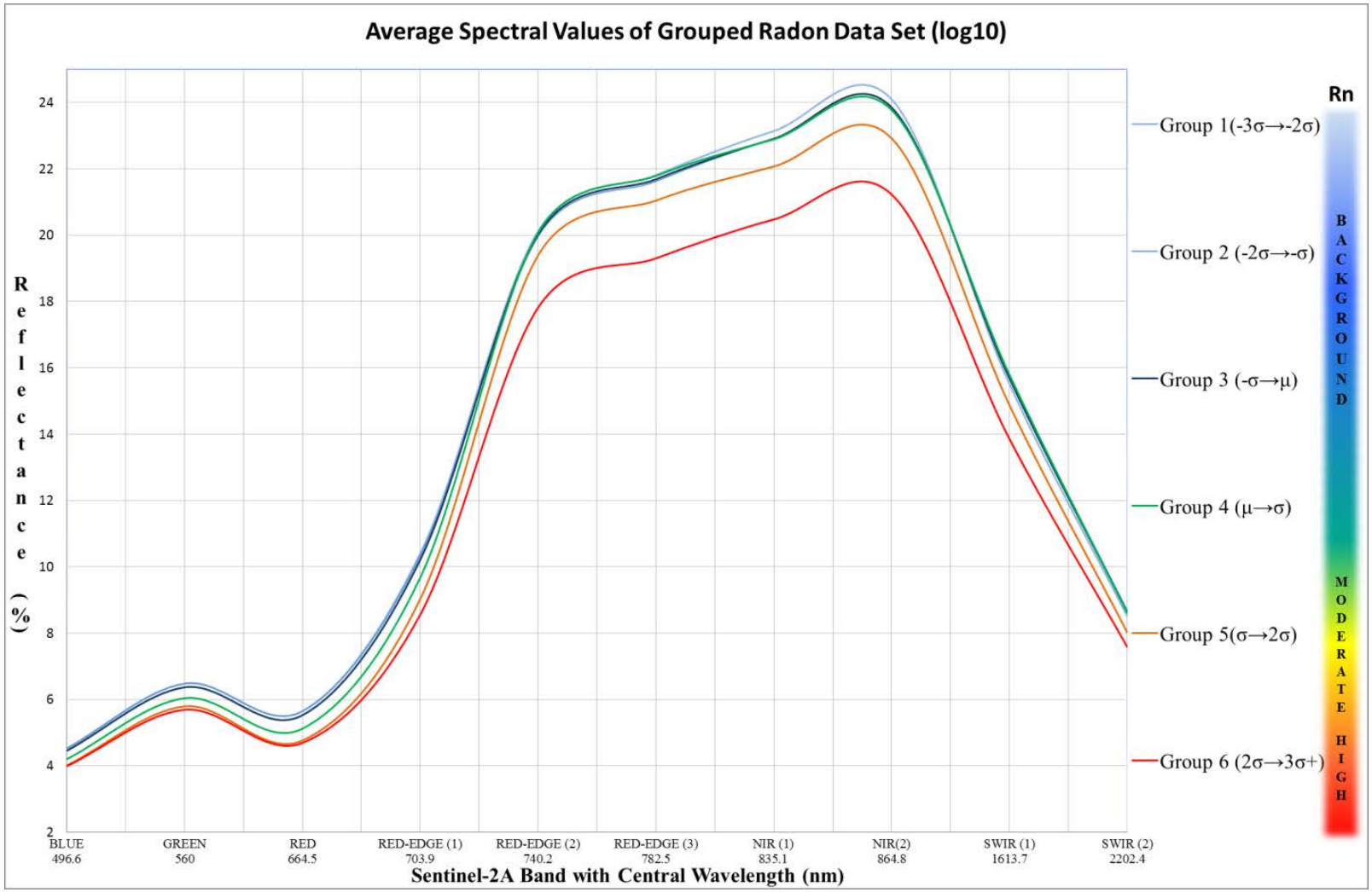

Figure 6-8 Average reflectance of each group of radon values for Sentinel-2A bands.

6.5 Trend Detection

The average value of select vegetation indices for each group was generated in order to maximize the difference observed in the spectral curves, specifically highlighting variation between the red-edge and NIR portion of the spectrum. Correlation and regression analysis was performed between the mean index values for each of the six radon groups. Coefficients of determination show the most significant relationships occur between the grouped radon data and RNVI2 and TCVI indices as they explain 91% and 90% of the variability in the differences of means therein, respectively (Table 6.7-1).

Table 6.7-1 Coefficients of determination statistics for mean vegetation indices and radon group

	r^2	*a*	t-stat *a*	p-value *a*	*b*	t-stat *b*	p-value *b*
TCVI	0.90	-108	-8.95	0.01	18.4	5.94	0.00
RnVI(1)	0.47	17.1	29.8	7.54e-06	-0.28	-1.88	0.13
RnVI(2)	0.91	-116	-13.1	0.00	14.7	6.49	0.00
CVI	0.18	0.18	0.073	1.52e-06	-0.02	-0.94	0.40
ClRed-edge	0.76	0.19	27.8	9.98e-06	0.04	3.59	0.02

The TCHVI and RNVI(2) scatter plots show a similar overall trend; the sharpest transformation appears to occur between the second and third group ((−2σ→-σ) and (−σ→μ)) and the fourth and fifth group ((μ→ σ) and (σ→2σ)) (Figure 6-9). The spectral curve observed in the previous section showed groups one through four to be operating on similar trends, essentially representing what can be considered background levels of radon gas in the environment. Here, it is shown there is more of a difference between background and moderate levels of radon gas and there is a plateau between moderate and strong amount of radon represented in groups five and six.

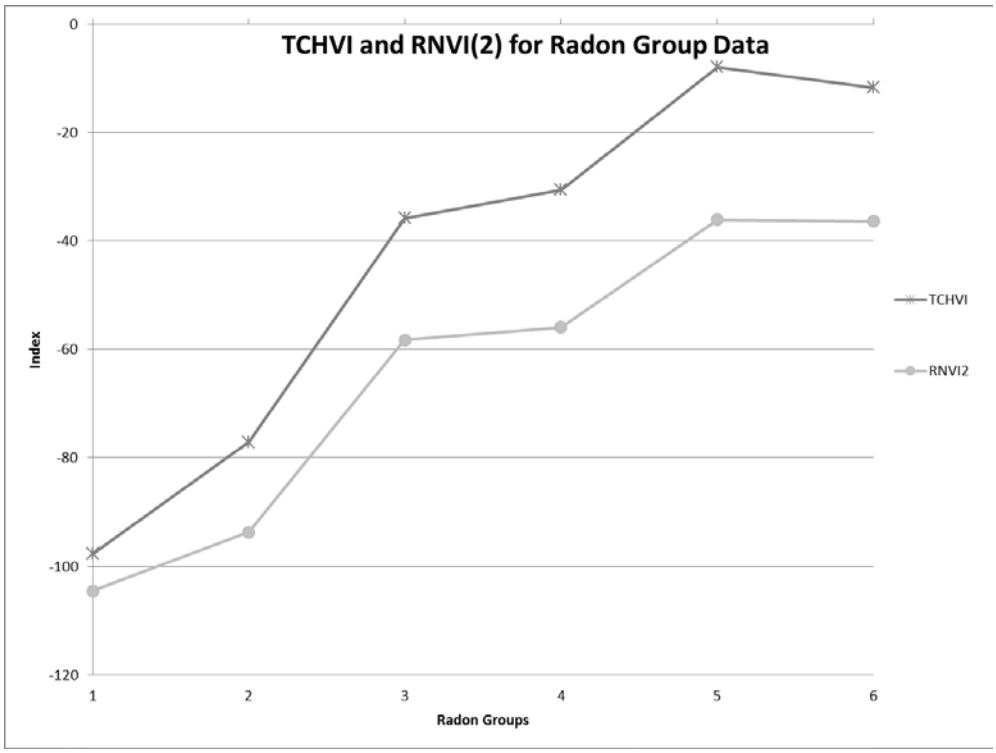

Figure 6-9 Scatter plot of radon groups and corresponding indices means (TCHVI and RNVI(2)) radon groups.

6.6 Radon Pseudo-Survey Map

Efforts were made to generate radon pseudo-survey maps using the indices that showed the highest r^2 values, specifically TCHVI and RNVI(2). The resulting maps showed poor visual correlation with elevated clusters of radon presumably due to the most significant change being between groups considered to be background levels of radon gas. Finally, a map was generated using the RNVI(1) indices that, during the trend detection analysis, showed a weak to moderate r^2 value (0.47) and weak linear trend. Plots of the index roughly show a similar range for groups one through five, and a stark decrease in values for what is considered anomalously high values of radon (Figure 6-10A). A moderate negative linear trend is observed between background, moderate, and high values of radon gas (Figure 6-10B).

A

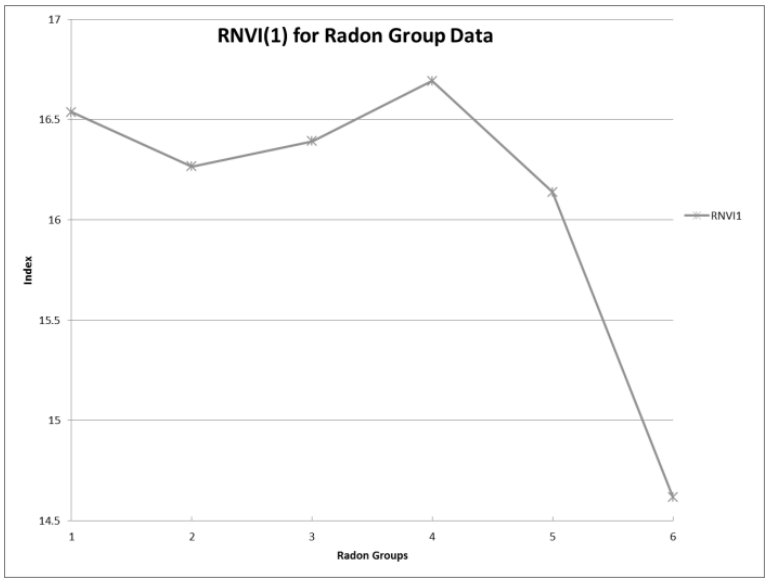

B

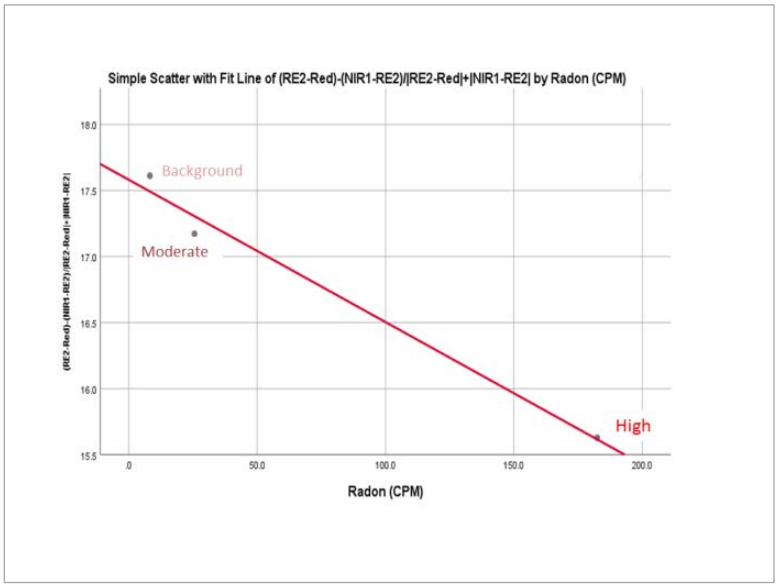

Figure 6-10 A) Scatter plot for radon groups and RNVI(1) index. B) Scatter plot of radon values vs grouped RNVI(1) index values for background, moderate, and high values of radon gas.

A map, with 20 m^2 spatial resolution, was then generated using the RNVI(1) index (Figure 6-11). The color profile of the modelled Sentinel-2A image was clipped to show index values between seventeen and ten. Due to the negative correlation between the index and radon values, as the index values decrease they are representing an increase in radon values.

Visually, there is a strong correlation between the anomalous clusters of radon, specifically in the Janine, AR, and AQ areas (Figure 6-11). The radon pseudo-survey map has generated a similar profile with the same approximate boundaries and consistent sigmoidal shape as radon point value clusters (Figure 6-11).

Various types of known radioactive anomalies and uranium showings are also plotted on the map, both with and without radon survey coverage. Outside of the area with plotted radon values, specifically to the north, the radon pseudo-survey map successfully highlights the ZH uraniferous showing. There is also a scatter of slightly anomalous pseudo-survey response is also shown that correlates well with a zone of weak "radioactive anomalies" (ie ZD zones 1→3, Figure 6-11).

A broad-scale pseudo-survey map, without radon points superimposed, highlights regional trends as well as known uraniferous, geochemical, and/or radiometric anomalies on the Cluff Lake property (Figure 6-13). The orebodies have been mined out of the ground and reclaimed; therefor they do not provide the same index response within the pseudo-survey map. Surficial contamination from mining activities also creates scatter within the radon pseudo-survey, predominantly in areas with a high concentration of infrastructure, such as the area directly north of Cluff Lake proper. Overall, strong visual correlation with radon-source locations is shown.

Anthropogenic and natural fluctuations within vegetation communities, attributed to mining and forest fire activity, will influence the capacity of the survey. For example, the northeast portion of the Janine anomaly in the pseudo-survey map does not indicate the same strong levels of radon as shown by the radon point values (Figure 6-12). Analysis of the higher resolution WorldView2 data interpreted this to be the result of relict east-west trending cut-lines that remain in the area. This is a clear indication that the anthropogenic activity has changed the vegetation and therefore also affected the range of index values indicative of an anomaly within the pseudo-survey map.

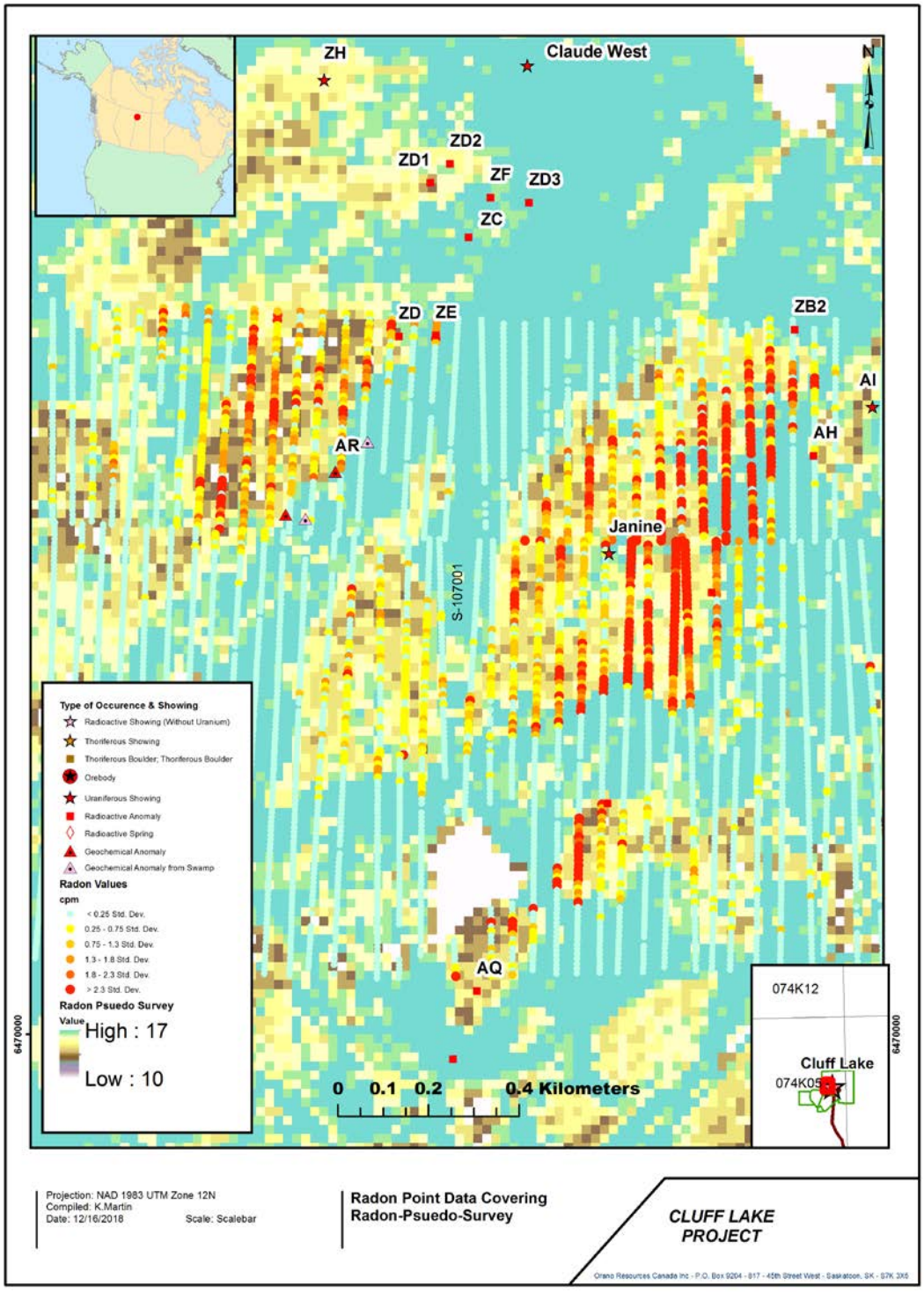

Figure 6-11 Radon-pseudo-survey map generated using RNVI (1) index overlain with radon point values plotted based on variation in standard deviation (Sentinel-2A). The dominant light blue color represents the highest end of the selected range and equates to

background levels of radon gas; as the index transitions to lower values, towards warmer colors yellow and brown, the map is highlighting moderate to high values of radon gas. The radon point values are plotted according to their standard deviation; light blue represents the lowest values and red represents the highest.

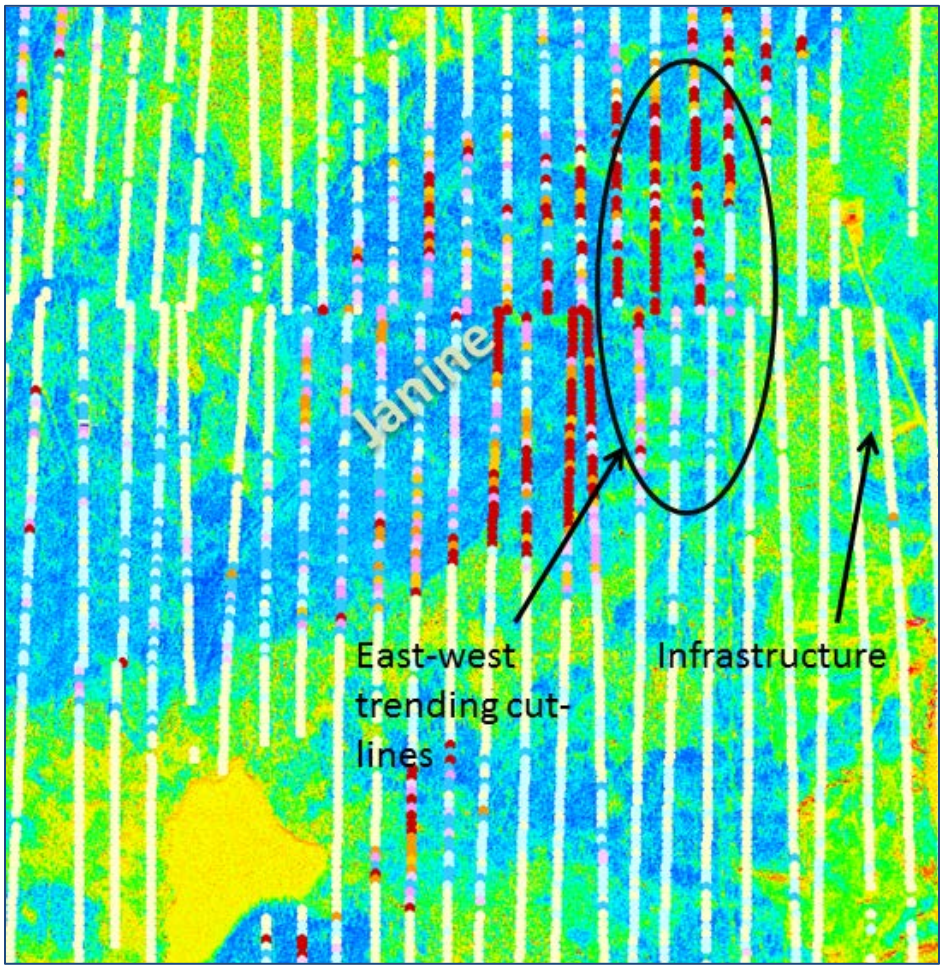

Figure 6-12 Worldview pseudo color image of the red-edge band highlights the cut lines and infrastructure in the northeast portion of the Janine radon anomaly that has interfered in radon-pseudo-survey map generation.

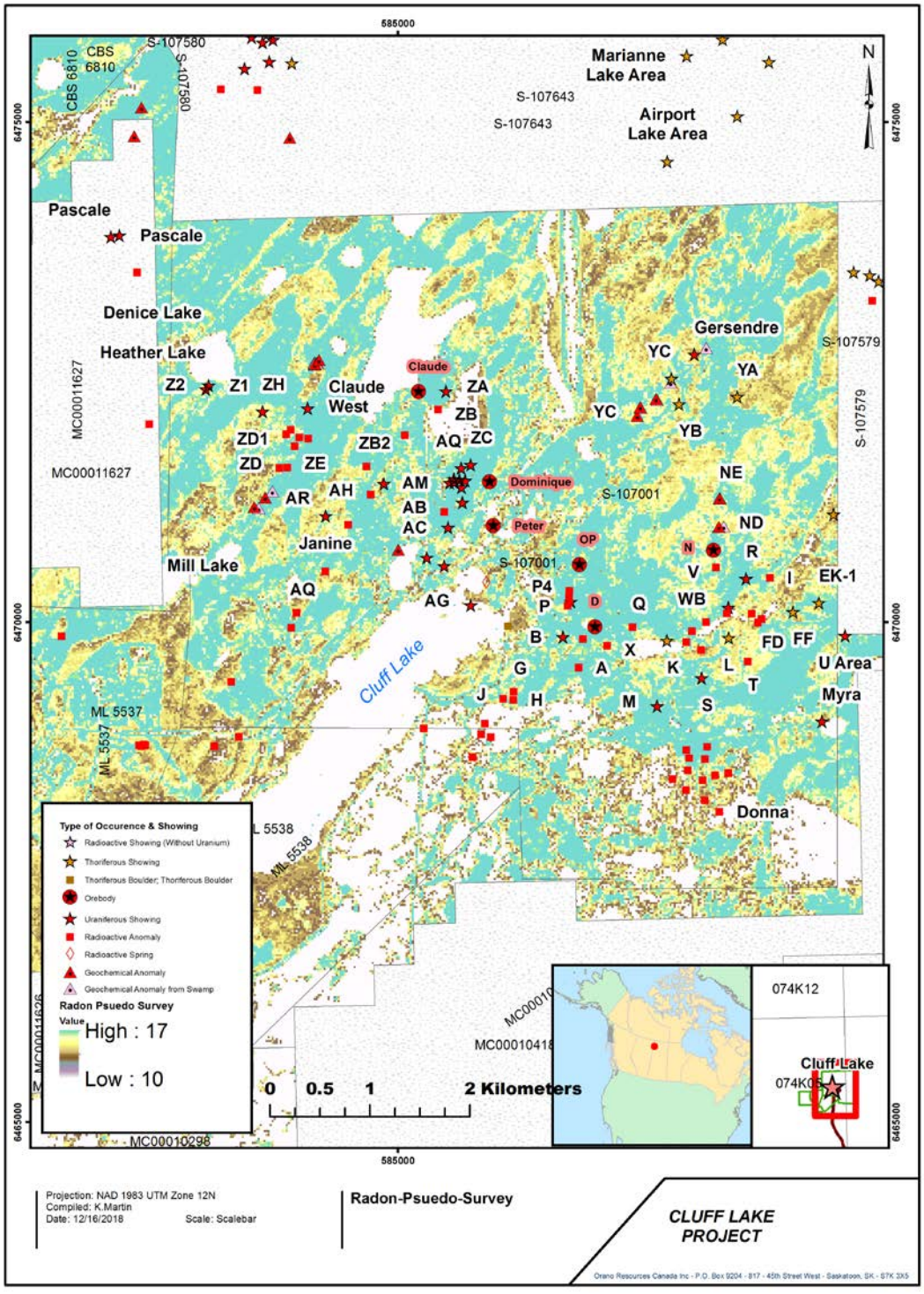

Figure 6-13 Regional scale radon pseudo-survey map generated using RNVI (1) index (Sentinel-2A)*Spatial resolution of 20 meters.

7 Discussion

7.1 Radon Distribution

This research was entirely data-driven with the end objective of increasing knowledge pertaining to spectral signature characteristics of vegetation exposed to radon gas as well as establishing a method of mapping radon from a satellite platform. The first phase of research focused on understanding the spatial distribution of radon gas at Cluff Lake, Saskatchewan. This formed a foundation for the remote sensing work and allowed for mechanistic explanation(s) of the results to be formulated.

Correlation analysis among soil gases, vegetation classes, and environmental gradients such as elevation were investigated generally yielding weak to no relationships with radon gas values. It was initially expected to see vegetation communities varying spatially with topographic relief as it determines factors such as moisture, slope, and exposure to light which are important factors in vegetation community dynamics. At the scale of this study, there were no correlation observed between vegetation communities and topography.

One relationship of potential significance that was not hypothesized corresponded with radon and black spruce distribution. It is generally accepted that black spruce tend to occupy low wet areas such as muskegs and bogs (Hogan, 2008). It was noted in the 1978 vegetation classification survey that black spruce tended to be present in poorly drained sites and were generally visibly stunted, however, the overall shape and size of the community class did not align with elevation contours. The generalization that black spruce are only found in low wet areas does not take the full range of species variability and all potential ecosystem processes into consideration. Patterns in black spruce community composition are complex and largely depend on species-subtype and scale; they arise in response to a hierarchy of environmental variables including, but not limited to, regional-scale variation in pH, local paludification (peatland formation) variances, and fine-scale differences in topography and drainage (Hollingsworth, 2006). Interestingly, biogeochemical surveys performed in the late 1970's and early 1980's found that black spruce were generally the best species to sample as they consistently assayed the highest amounts of uranium within its twigs and needles (Dunn, 1980).

This raises the question of whether black spruce is better suited to absorbing and storing uranium than other coniferous species, or, alternatively if there is a preference for black-spruce-dominant-vegetation-communities to occupy areas that have elevated radiogenic activity?

Existing scientific literature shed light on these questions. It is known that the effects of gamma irradiation within conifers differ significantly among species (El-Lakany, 1970). Vegetation stresses are the immediate response to environmental stimuli including mechanisms of tolerance and resistance (Arnholt-Schmitt, 2004). To accommodate stress, plants often initiate acclimation and adaptation processes (Hermans *et al*., 2006; Hikosaka *et al*., 2006). These processes involve immediate and long-term modifications to metabolic processes so that changing environmental conditions can be met (Baena-González, 2010). Vegetation communities are dynamic yet the possibility exists that adaptive response mechanisms operate where black spruce has a competitive advantage within vegetation communities that have been exposed to chronic radiation doses at Cluff Lake.

Ecological and evolutionary perspectives were also considered. Until recently, evolutionary processes were generally thought to be acting on longer time scales than ecological processes that shape ecosystem architecture (Eriksson, 2014). Vegetation community assembly and composition, specifically at Cluff Lake, has likely been strongly influenced by environmental factors such as the presence of shallow uranium mineralization that formed over one-billion years ago; significantly pre-dating plant life on land. It is plausible that variation of surficial radiation levels may have significantly influenced the establishment of the paleo-ecosystem. When a population is exposed to radiation over multiple generations, natural selection may favor more radioresistant-genotypes and, thereby, gradually increase the mean tolerance of the population via radioadapation (Stanislav, 2016). Radioadaptation mechanisms within plants depend on two factors: species flexibility including dispersal, intra-population variability, and physiology, and the type and level of environmental contamination including dose rate, internal or external radiation sources, and other ecological factors able to modify effects of radiation (Stanislav, 2016). Ultimately, it is reasonable to hypothesize that black spruce has preferentially populated areas with elevated occurrences of radiogenic material due to genetic mutations over thousands of years.

The relationship between black spruce and radon gas merits further ecological research. Understanding response mechanisms within ecosystems and plant populations is complex, dynamic, and beyond the scope of this paper. If a species-specific relationship between black spruce and radon gas exists, further study of the ecological relationship between community compositions mediated by radiation dose will be pivotal to further understanding the spectral signature attributed to radon gas within vegetation specific to the boreal forest ecosystem.

7.2 Radon Detection via Optical Remote Sensing

The plotted spectral curves, consisting of all Sentinel-2A bands, show a clear difference among what is considered low, moderate, and high radon values. The most notable variation is within the NIR portions of the electromagnetic spectrum where the high radon values are represented by the lowest reflectance (Figure 6-8). This observation is thus primarily attributed to stress characteristics within vegetation associated with the radiogenic properties of the gas and/or contamination from its metal progeny. Lower reflectance values within vegetation are often attributed to lower chlorophyll content. This has been shown to be the case in vegetation that has been subjected to toxic levels of heavy metals (Horler *et al*., 1980, 1983), and could explain the phenomenon observed here. Furthermore, a radon pseudo-survey map was generated using the RnVI(1) index that showed reasonable statistical and visual correlation with anomalously high clusters of radon gas at Cluff Lake.

7.3 Research Contributions

A significant amount of legacy data was digitized in conjunction with this study. Geo-referencing and digitization of historic maps has a way of breathing new life into work of otherwise limited value. Revisiting historic data with the capacity for detailed geo-spatial analysis is a powerful platform for innovation and exploration of relationships that would otherwise go undetected.

The interaction between radon gas and vegetation remains poorly understood. There is potential that incorporating vegetation transportation mechanisms into radon surveying techniques could increase the effectiveness of radon surveys and hypothetically increase depth of resolution, which has been a primary limitation of current survey methods. Vegetation stress responses to

chronic radon exposure are relatively constant and consistent compared to radon concentration as the gas is diffuse and volatile in nature but also depends on environmental variables such as moisture content and barometric pressure for accurate sampling. Hence, using a spectral signature derived from vegetation in surveying techniques, either primary or supplementary, would provide an effective, cost and time efficient, and environmentally low-impact method for current radon survey techniques.

This research has contributed to the understanding of spectral curve variation within vegetation as it applies to radon gas concentration; successfully differentiating between background and elevated occurrences of radon gas. Two indices have been proposed with the ability to predictively map for radon gas in "radon-pseudo surveys" that have been applied to areas outside of the boundary of available radon gas values. These show moderate statistical and good visual correlation with known uranium showings and geochemical anomalies in the Cluff Lake area.

This research has successfully contributed to an understanding of how optical remote sensing can be used to detect radon gas within vegetation. Great potential exists for building upon this work and further refining a tool that can be used in areas such as uranium exploration and environmental monitoring.

7.4 Research Limitations

A substantial portion of the pertinent data available for this study was georeferenced from historic maps with unknown associated recording error. It is estimated that up to 50 meters of error may exist for the geo-referenced radon point data. The data, though messy, remains useful for initial exploration of study areas and hypothesis generation (Miller, 2015), however, the uncertainty of these observations limits the accuracy of the results. Additionally, it has been assumed that the data collected in the late 1970's has not changed. The historic radon data were partially validated by the 2016 survey, and it is accepted that the vegetation classification data from the same era has been unchanged due to the protection of the mine site from forest fires for the past 40 years.

To run statistical analyses on the spectral characteristics of varying amounts of radon gas within the Sentinel-2A imagery, the data sets were joined. The data was complete with over 40,000 points, posing big-data limitations and the need to categorize data in bins. Data was natural-logarithmically transformed and partitioned in to six groups based on one standard deviation above and below the mean so that spectral curves could be generated for comparison. This permitted a closer approximation to the normal distribution and made the variability between groups more constant. The transformed and subsequently grouped data, when analyzed, showed a marked improvement in trend detection and statistical correlation analysis compared to non-transformed analysis. Performing data transformations can add to the uncertainty of the results, however the large volume of data improves the power of scaling. Generally, big data analysis is used as a tool to inform, rather than explain (Cukier, 2013). Data-driven approaches can lead to knowledge discovery, but should be used with caution. It is important to ensure models are both true and understandable and not based on spurious patterns generated by correlation while ignoring causation (Miller, 2014). For the purpose of this work, and for the first past assessment of the effectiveness of optical remote sensing to detect radon within vegetation, digitizing and analyzing the large legacy data set was instrumental to establish several hypotheses for further research.

The development of the radon pseudo survey map comes with the primary assumption that correlation observed at Cluff Lake can be extrapolated to other areas. It is an understatement to say that natural systems are complex and multivariate. Unique geological and ecological factors, such as unconformity depth and vegetation community dynamics, will have to be considered when applying this newly developed tool in other areas. This study, as it was performed in a boreal forest ecosystem, is constrained to vegetation communities therein; applying the technique outside of the boreal forest system will introduce a new set of variables and may be a topic for further research.

The exact spectral characteristics of radon's effects in plant physiology require further research across varying vegetation communities. Ground truthing of the pseudo-survey is required to validate the research. Based on the spectral characteristics of the grouped radon data and the

strong correlation of determination between vegetation indices such as TCHVI and RNVI(2), strong potential for using spectral characteristics within vegetation to quantify radon levels exist.

7.5 Applications

Imaging radon gas via spectral properties of vegetation has important applications for uranium exploration. Current radon survey methods are generally considered effective for uranium plays with shallow depth potential, with a maximum depth of uranium mineralization at approximately 150 meters. Applying this remote sensing technique should follow the same guidelines; at least until the resolution depth is better understood. Additionally, this technique should only be considered valid within boreal forest ecosystems until studies in other environments have been performed. The research has trans-disciplinary applications in biogeochemistry, ecology, and the environmental sector. Outside of uranium exploration, a primary application would be in uranium mine-site reclamation and or environmental monitoring of nuclear facilities. This method allows for fast, large scale, and inexpensive assessment of radiogenic contamination and allows for detailed time-series studies to be performed in reclamation areas.

7.6 Recommendations

A study with a more rigorous set of controls should be formed, potentially in a green house or laboratory setting, allowing variables to be isolated. This way, the precision and resolution of the spectral variation suggested in this study can be investigated in greater detail.

Field trials are also recommended to improve spectral mapping capabilities of radon gas in natural systems. The initial work should focus on generating reference spectra between black spruce from: 1) areas of highly anomalous radon concentration, and 2) in areas that are considered to have background levels of radon gas. Ultimately, the detailed spectral curve of black spruce exposed to chronic high-levels of radiation should be compared to black spruce in background levels of radon gas in great detail. Additionally, the vegetation selected for generating reference spectra should bio-geochemically sampled and assessed for heavy metal concentration.

In areas where there is no radon ground survey coverage, it is recommended to use the pseudo-survey-map to highlight areas of potential anomalous radon and that can be followed-up with ground surveys in order to test the results.

As this study is focused within the boreal forest of Northern Canada, it is also recommended for further studies of the effect of radon gas within varying vegetation communities and ecosystems in order to establish a more global understanding of the application of this tool.

8 Conclusion

Results indicate a significant and map-able variation in Sentinel-2A spectra responses between what is considered to be background and elevated levels of radon within vegetation in a boreal forest ecosystem. It is observed that vegetation within clusters of radon-highs show a marked decrease in reflective values, predominantly in the red-edge and NIR regions. This indicates a physiological response interpreted to result from radiogenic stress and, by proxy, heavy metal contamination.

Understanding the capabilities of optical remote sensing as a tool to detect elevated occurrences of radiogenic material such as radon gas is in its infancy. This research is intended to provide an initial assessment of its utility, specifically for the uranium exploration industry. This research shows that strong potential exists for using optical remote sensing for quantifying radiogenic stress within vegetation as well as creating and refining predictive models to map the spatial variation of radon gas in the environment.

9 REFRENCES

Amok (1978). Surface Geology of the Carswell Structure. Internal Report, Orano Canada Inc., Cluff Area Chronological (146).

AREVA (ORANO Canada) (2001) Comprehensive study for decommissioning, Areva Resources Canada Inc.

Arnholdt-Schmitt, B. (2004) Stress-induced cell reprogramming: a role for global genome regulation. Plant Physiology, 136 (2004), pp. 2579-2586.

Baena-González, E. (2010). Energy signaling in the regulation of gene expression during stress. Mol. Plant., 3 (2010), pp. 300-313.

Barton, C. (2012). Advances in remote sensing of plant stress. Plant and Soil, Vol354(1), pp.41-44.

Baskaran M. (2016) Radon: A tracer for geochemical exploration. In: Radon: A Tracer for Geological, Geophysical and Geochemical Studies. Springer Geochemistry. Springer, Cham.

Bell, K. (1985). Geochronology of the Carswell area, northern Saskatchewan. *In* The Carswell Structure Uranium Deposits, Saskatchewan. Geological Association of Canada, Vol. 29, pp. 34–46.

Bleeker, W. *et al*. (2015): The age of the Carswell impact structure. AGU-GAC-MAC-CGU Joint Assembly, Montreal Quebec, May 3-7 2015, Abstracts Listing, v. 38, p. 341.

Card, J.W., Bell K. (1982). Collection of radon decay products – a uranium exploration technique. Journal of Geochemical Exploration 17(1):63-76.

Clevers *et al*. (2004). Study of heavy metal contamination in river floodplains using the red-edge position in spectroscopic data. International Journal of Remote Sensing, 25(19) 3883-3895.

Davids & Tyler, (2002). Detecting contamination-induced tree stress within the Chernobyl exclusion zone. Remote Sensing of Environment 85 (2003) 30–38.

Dunn, C.E., (1980). The biogeochemical expression of deeply buried uranium mineralization in Saskatchewan, Canada. Proceeding of 8th Int. Geochemical Exploration Symposium (Hannover, Germany, April, 1980), Assoc. Explor. Geochemists.

Dunn, C.E., (2007). New perspectives on biogeochemical exploration. Advances in Prospect-Scale Geochemical Methods. In “Proceedings of Exploration 07: Fifth Decennial International Conference of mineral Exploration” edited by B. Milkereit, p.249-261.

El-Lakany, M.H., O. Sziklai, O. (1970). Effects of gamma radiation on some western conifers. Radiation Botany.Vol. 10, pp. 411 to 420. Pergamon Press. Printed in Great Britain.

Eriksson, Ove. (2014). Vegetation change and eco-evolutionary dynamics. Journal of Vegetation Science 25 (2014) 1141-1147.

Gurau D., Stanga D., Dragusin M., (2014). Review of the principle mechanism of radon. Romanian Journal of Physics, 59, 904-911.

Harley, Naomi H., Chittaporn, Passaporn, Fisenne, Isabel M., (2017) Seismic prediction using unattached radon decay products. Radiation Protection Dosimetry, 177(1-2):160–163.

Hermans C, Hammond JP, White PJ, Verbruggen N., (2006) How do plants respond to nutrient shortage by biomass allocation? Trends Plant Sci., 11:610-617.

Herrmann, I.; Pimstein, A.; Karnieli, A.; Cohen, Y.; Alchanatis, V.; Bonfil, D.J. (2011). LAI assessment of wheat and potato crops by VENμS and Sentinel-2 bands. Remote Sensing of Environment, 115 (8):2141-2151.

Hikosaka K., Ishikawa K., Borjigidai A., Muller O., Onoda Y., (2006). Temperature acclimation of photosynthesis: mechanisms involved in the changes in temperature dependence of photosynthetic rate. J. Exp. Bot., 57:291-302

Hogan, C. Michael (2008). Stromberg, Nicklas, ed. Black Spruce: Picea mariana GlobalTwitcher.com (March 13, 2019).

Hollingsworth, T.N.; Walker, M.D.; Chapin, F.S., III; Parsons, A.L., (2006) Scale-dependent environmental controls over species composition in Alaskan black spruce communities. Canadian Journal of Forest Research; Ottawa. 36 (7)1781-1796.

Horler *et al*. (1983) The red-edge of plant leaf reflectance. International Journal of remote sensing, 4:273-288.

Huxtable, D., Read D., Shaw G., (2017). Measuring radon-222 in soil gas with high spatial and temporal resolution. Journal of Environmental Radioactivity 167, 36e42.

Jayarante *et al*., (2011). Role of vegetation in enhancing radon concentration and ion production in the atmosphere. Environmental Science and technology.

Koning, E., (2013): The Cluff Lake Project (Claim S-107001) History of exploration work and remaining uranium potential. Orano Canada Inc. Internal Report Number 13-CND-97-01.

Kozak, Alexander Joseph; Reeves, Howard William; Lewis, Barbara Ann. (2003). Modelling radium and radon transport through soil and vegetation. Journal of Contaminant Hydrology 66, 179-200.

Kyser, K., and Cuney, M., (2008). Unconformity-related uranium deposits. Mineralogical Association of Canada. Short Course Series, Vol. 39, Mineralogical Association of Canada, Que., pp. 7–95. Google Scholar.

Malimo, S.J., (2012). Use of radon and carbon dioxide in geochemical exploration of Menengai and Silali geothermal prospects, Kenya. Proceedings of the 4th African Rift Geothermal Conference 2012 Nairobi, Kenya, 21-23 November 2012.

Miller, Harvey J., (2014). Data-driven geography. GeoJournal (2015) 80:449-461. Published online: 10 Oct 2014.

Orano, (2018). 2018 Cluff Lake assessment report. Internal Report 18-CND-97-01, Orano Canada Inc.,

Ortega, M.F.*et al*., (2014). Gas monitoring methodology and application to CCS projects as defined by atmospheric and remote sensing survey in the natural analogue of Campo De Calatrava. Global NEST Journal, 16 (2), 269-279.

Pacer, J.C., and Czarnecki, R.F. (1980). Principles and characteristics of surface radon and helium, techniques used in uranium exploration. Benxix Feild Engineering Corporation, Colorado. Prepared for U.S. department of Energy (GJBX-177(80)).

Pinault &Baubron, (1996). Signal processing of soil gas radon, atmospheric pressure, moisture, and soil temperature data: a new approach for radon concentration modelling. Journal of Geophysical Research, VOL.101, No.B2, Page 3157-3171, February 10,1996.

Powell, B., (1985). Case histories of the radon tube sampler in the Carswell structure. The Carswell structure uranium deposits, Saskatchewan. Geological Association of Canada Special Paper; 29. ISBN 0-919216-27-7.

RadonEx, (2015). EIC surveys, Accessed Sept 27 2015. http://www.radonex.com/eic-surveys/.

Ramola, *et al*., (1989). Geochemical exploration of uranium using radon measurement techniques. Nuclear Geophysics; 3(1):57-69.

Rock *et al.*,(1986). Remote Detection of Forest Damage Author(s): B. N. Rock, J. E. Vogelmann, D. L. Williams, A. F. Vogelmann and T. HoshizakiSource: BioScience, Vol. 36, No. 7, Ecology from Space (Jul. - Aug., 1986), pp. 439-445Published by: Oxford University Press on behalf of the American Institute of Biological Sciences.

Ruhlmann, F., (1985). Mineralogy and metallogeny of uraniferous occurrences in the Carswell structure: in the Carswell structure uranium deposits, Saskatchewan. Geological Association of Canada, Vol. 29, pp. 105–120.

Seager, S.,(2002). The vegetation red edge spectroscopic feature as a surface biomarker S. Seager (DTM/CIW), E.B. Ford (Princeton), Astrophysics of Life conference proceedings, STScI May 2002, 9 pages, arXiv:astro-ph/0212550v1.

Walia, V., Su, T.C., Fu, C.C., Yang, T.F. (2005). Spatial variations of radon and helium concentrations in soil-gas across the Shan-Chiao fault, Northern Taiwan. Radiation Measurements 40, 513-516.

Yefremenko V.V., *et al*. (1998). Use of false color scanner imagery to detect vegetation stress. Mapping Sciences and Remote Sensing, 1998, 35:3, 218-226.

10 APPENDIX A: Sentinel 2A Imagery

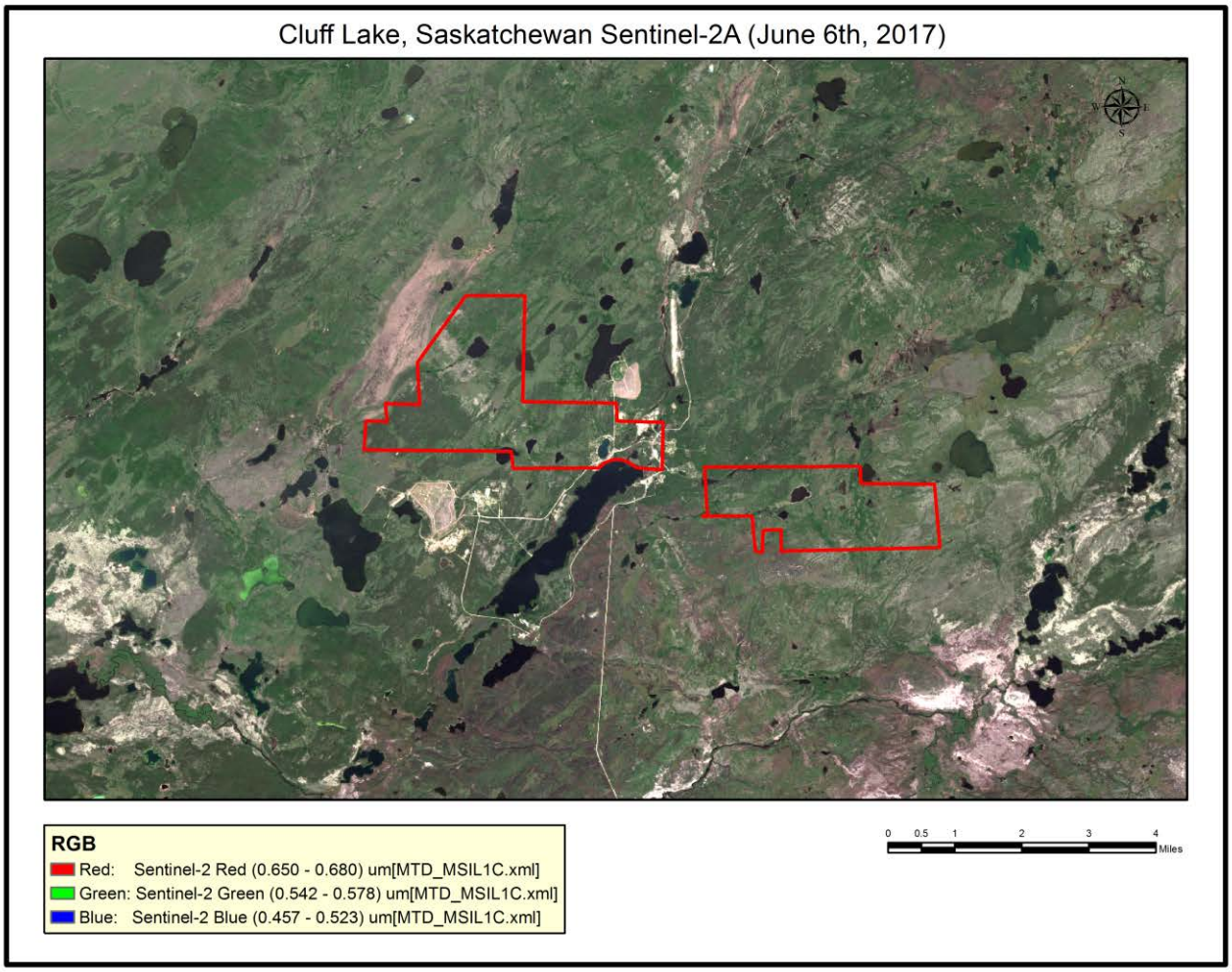

11 APPENDIX B: WorldView-2 Imagery

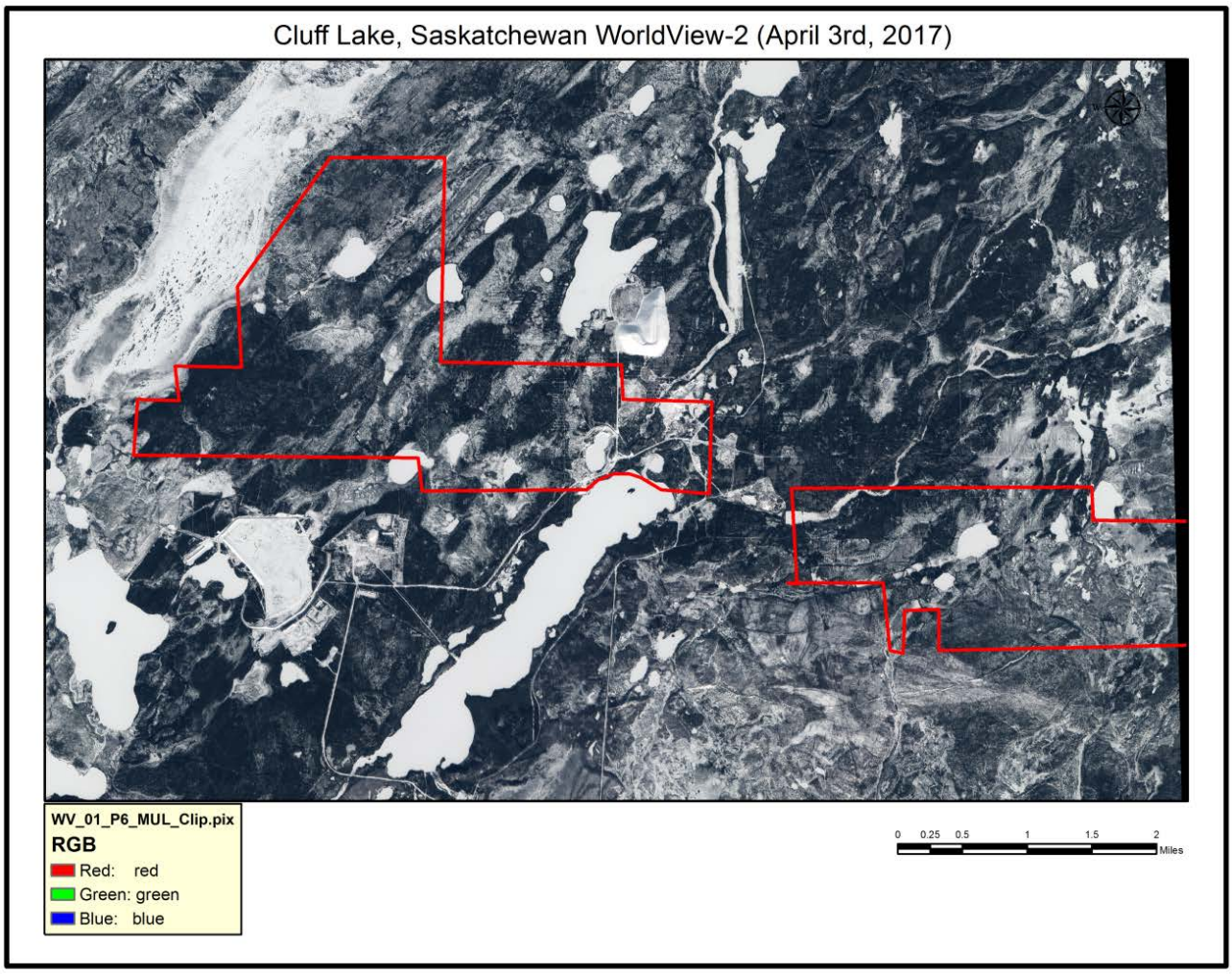

12 APPENDIX C: Geology Map of the Carswell Structure